A MODEL PREDICTIVE CONTROL STRATEGY BASED ON PREDICTED MEAN VOTE FOR A BUILDING HVAC SYSTEM

Mr. Chanthawit Anuntasethakul

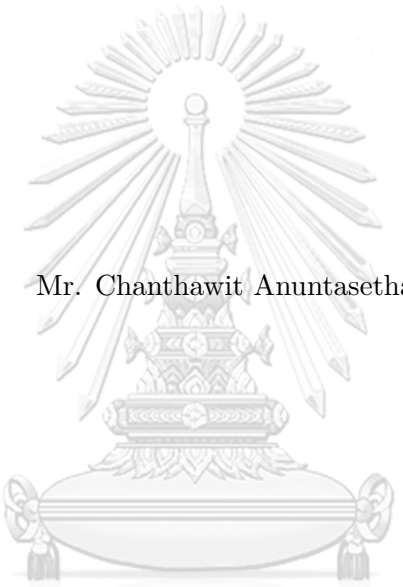

A Thesis Submitted in Partial Fulfillment of the Requirements
for the Degree of Master of Engineering Program in Electrical Engineering
Department of Electrical Engineering
Faculty of Engineering
Chulalongkorn University
Academic Year 2020

Thesis Title	A MODEL PREDICTIVE CONTROL STRATEGY BASED ON PREDICTED MEAN VOTE FOR A BUILDING HVAC SYSTEM
By	Mr. Chanthawit Anuntasethakul
Field of Study	Electrical Engineering
Thesis Advisor	Professor David Banjerdpongchai, PhD

Accepted by the Faculty of Engineering, Chulalongkorn University in Partial Fulfillment of the Requirements for the Master's Degree

..... Dean of the Faculty of Engineering
(Associate Professor Supot Teachavorasinskun, D.Eng.)

THESIS COMMITTEE

..... Chairman
(Assistant Professor Manop Wongsaisuwan, D.Eng.)

..... Thesis Advisor
(Professor David Banjerdpongchai, Ph.D.)

..... Examiner
(Assistant Professor Sunhapos Chantranuwathana, Ph.D.)

..... External Examiner
(Associate Professor Waree Kongprawechnon, Ph.D.)

(A MODEL PREDICTIVE CONTROL STRATEGY BASED ON PREDICTED MEAN VOTEFOR A BUILDING HVAC SYSTEM),

##617 01318 21: MAJOR ELECTRICAL ENGINEERING
KEYWORDS: HEATING-VENTILATION-AIR-CONDITIONING (HVAC) / MODEL PREDICTIVE CONTROL (MPC) / PREDICTED MEAN VOTE (PMV) / PEAK-LOAD SHAVING / SUPERVISORY CONTROL (SC).

CHANTHAWIT ANUNTASETHAKUL: A MODEL PREDICTIVE CONTROL STRATEGY BASED ON PREDICTED MEAN VOTE FOR A BUILDING HVAC SYSTEM. ADVISOR: PROFESSOR DAVID BANJERDPONGCHAI, Ph.D., 81 pp.

This thesis proposes a design of a supervisory model predictive controller for a heating-ventilation-air-conditioning (HVAC) control system. The control objective is to minimize the operating cost and take into account of electrical load shaving and thermal comfort of users. To ensure that thermal comfort is well regulated, we utilize the Predicted Mean Vote (PMV) as an indicator and determine an acceptable bound of a desired set-point temperature. The control design consists of two layers, namely, a supervisory control (SC) layer and a model predictive control (MPC) layer. For the SC layer, we explore a configuration including the choice of predesign controller, the analysis of steady-state response, and the possible range of the set-point temperature. We incorporate the effect of set-point temperature, air velocity, outside air temperature, heat load inside zone onto the HVAC electrical power. Then, we search for an optimal profile of the set-point temperature that minimizes a weighted sum of a total operating cost (TOC) and a thermal comfort cost (TCC). Moreover, exploration of trade-off between TOC and TCC helps us to achieve both control objectives efficiently. For the MPC layer, we formulate the control design with the objective of tracking the optimal set-point temperature and minimizing the control inputs. We apply the proposed control design to a complex dynamical model of HVAC system with volumetric flow rate, electrical power of heat exchanger, and removed moisture as control variables and test with various weather conditions. When the allowable PMV of the zone is specified within a certain comfort level, the TOC of the proposed supervisory MPC is significantly reduced compared with that of the nominal operation. The maximum electricity demand of HVAC system is reduced and the electrical power profile is smoothly shaved. Fur-

thermore, the zone relative humidity is well regulated and corresponds to the operating condition of the SC layer.

Department: .. Electrical Engineering ..	Student's Signature .....
Field of Study: . Electrical Engineering .	Advisor's Signature .....
Academic Year 2020	

ACKNOWLEDGEMENTS

A thesis can be said to be a complete edition of a person's work. It summarizes the idea, concept, and personalization of the writer and cannot be done by oneself. Without these people, this thesis cannot be said to be successfully completed.

First and foremost, I would like to express my best gratitude to my advisor, Professor David Banjerdpongchai, who supervised me since I was an undergraduate. Both his comments and his perspectives inspire me to do the research at my best.

Secondly, I am thankful for the chairman and all thesis committees including Assistant Professor Manop Wongsaisuwan, Associate Professor Sunhapos Chatranuwathana, and Associate Professor Waree Kongprawechnon for their willingness to become committees of this thesis and their suggestion to improve the quality of my work since the proposal examination.

Next, I am indebted to every lecturers in Control System Laboratory (CSRL), especially Assistant Professor Suchin Arunsawatwong and Assistant Professor Jitkomut Songsiri. During the classes and coursework, every lecturer gave me not only knowledge but also the way to think analytically.

I would like to say that Friendship never ends for all my friends and collaborators at Control System Laboratory (CSRL), Chulalongkorn University, especially, Poomipat Boonyakiatanon (Siya), Natthapol Techapgangam (Bank), Tadchanon Chuman (Bank), and Parinthorn Wanmanomai (Boss) for their kindness, support, and empathy. They always give warm consolation and encouragement and always help each other including me to pass the difficult time.

Last but not least, I would like to thank the family for their unconditional support and love. Until now, they always support me at their best although I'm the worst. The word "thank you" is never enough

CONTENTS

Chapter Page

LIST OF TABLES

LIST OF FIGURES

Figure Page

CHAPTER I

THESIS OVERVIEW

1.1 Introduction

Thailand electrical energy consumption is annually increasing influenced by Thailand economic growth. Gross Domestic Product (GDP) is one of the representatives of economic growth of a country. To demonstrate relationship between Thailand electrical energy consumption and Thailand GDP, Figure 1.1 shows Thailand energy consumption [1] versus Thailand GDP in 2010-2018 [2].

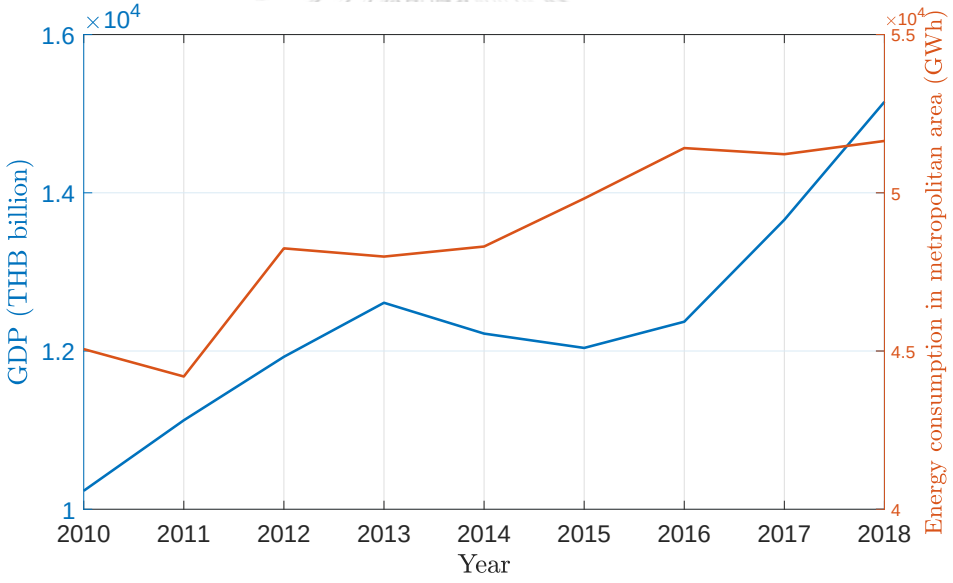

Figure 1.1: Thailand GDP and electricity energy consumption in 2010-2018.

From Figure 1.1, we can see that GDP and electrical energy consumption has the same tendency with a correlation = 0.81. Reported in [3, 4], this incident also happens in middle eastern countries and Italy. Not only the economic growth but also energy inefficiency is one of the major factors that leads to an increase of energy consumption [5, 6].

To improve this problem, upcoming technologies like intelligent control, smart

grid, and smart sensors [7] becomes a key to success since it allows us to precisely design and implement a large-scale energy management system.

An HVAC system is a common equipment for most buildings and is one of the largest energy consuming parts of the buildings. Energy consumption of the HVAC system depends on heat load and set-point temperature [8]. Since the set-point temperature of the HVAC system can be adjusted, it allows us to apply the HVAC system with the demand response strategies, which aims to organize users load profile and give them back an incentive payment rate [7].

Most studies in demand responses strategies for the HVAC system focus on only reduce energy consumption, thermal comfort condition for users is overlooked. Only few research focuses on the trade-off between thermal comfort and energy consumption [7, 9, 10]. Thermal comfort is a state of human feeling about their thermal satisfaction. Since thermal comfort is subjective to human feeling, Predicted Mean Vote (PMV) was developed by P.O. Fanger [11] which then standardized in ASHRAE55 [12]. Calculation of PMV involves temperature, humidity, air velocity, and users' parameters, for example, clothing index and users' activities.

Supervisory control (SC) is a management control layer which determine an operating condition for local controllers. The purpose of using the SC is scheduling and planning. For the problem formulation, the SC design can be formulated as an optimization problem. The optimal solution then becomes a set-point or operating condition for local controllers. In [13], there was a comprehensive review of using the SC with the HVAC control system.

Model Predictive Control (MPC), one of the advanced process control theories, is widely used in industrial process control system. The theories behind the MPC involves optimal control theories and numerical optimization [14]. The MPC is able to deal with both nonlinear and linear models and can handle various type of constraints. On the other hand, MPC always requires priori knowledge of the plant, for example, model parameters, operating parameters, and dynamic model.

Due to its ability to handle constraints, the MPC is widely used in chemical process, distillation process, and also HVAC system [15–19].

The application of the MPC to HVAC systems as intensively reviewed in [16]. Supervisory control design and time-varying set-point design was stated as challenging problems. It was suggested without illustrating that cost function of the controller can be composed of thermal comfort and energy saving. Reported in [17], a frequency control of air conditioning system was introduced. The authors integrated real-time pricing, performance mapping, and penalized error in the MPC problem. However, thermal comfort and humidity control are overlooked. In [18], appliance scheduling using MPC based on HVAC system and battery energy storage system was presented. ON/OFF control was integrated into the MPC problem whereas the cost function consists of time-varying energy cost and operating conditions. The authors also integrated PMV with the help of linear regression into the control design. Although the research was carefully conducted, we observe that lack of consideration of humidity and air velocity can adversely affect the approximation of the PMV. As results, thermal comfort might not be achieved. The MPC design with direct consideration of the PMV was presented in [19]. The authors solved the PMV-based optimization problem using their proposed method. As results, the authors successfully regulated temperature and PMV whereas energy consumption is reduced. However, they do not consider humidity control and peak-load shaving.

Recently, a few research focused on using a multi-layer controller to control HVAC systems. Supervisory Control and Data Acquisition (SCADA) system was used in energy management for HVAC system [20]. The local controller was selected to be programmable logic controller. Reported in [21], application of a cascaded control to the HVAC system was introduced. The authors applied the MPC for an outer control loop and used PID for an inner control loop. The MPC compute the set-point for the PID whereas the control objectives are to reduce energy consumption during off-peak hours. Energy price was regarded as time-varying function. As a result of their work, it suggested that set-point temperature adjustment has a significantly impact on the HVAC

electricity consumption. However, their design does not include effect of disturbances from internal load. Furthermore, they do not take comfort and humidity control into account of control design.

According to [22], the MPC and an open-loop controller are applied to HVAC control system. The open-loop controller defined an operating point of the HVAC system, The MPC then performed reference tracking and control input minimizing. The authors considered thermal comfort using ASHRAE comfort representation and translated it into temperature and humidity constraints. An extended version of this work can be found in [23]. Instead of finding operating conditions, the authors used an open-loop control to determine an optimal set-point for the MPC. The authors improved the MPC so that the cost function were composed of temperature regulation, humidity regulation, and CO_2 concentration regulation. However, we observe that there still has a research gap. The air velocity is not addressed in a calculation of thermal comfort. This might be resulted in violation of thermal comfort. In addition, both [22] and [23] do not consider peak-load shaving in their control design.

In this thesis, we propose a novel design of a supervisory MPC with application to HVAC system. Main control purposes are to regulation thermal comfort and to reduce total operating cost at the same time. We apply complex dynamic HVAC model including thermal system and humidity system with interactions among variables. We develop a computational-fluid-dynamic (CFD) model for our zone to approximate a profile of air velocity. In an SC layer, we introduce a set-point temperature design. The cost function is a weighted sum of total operating and thermal comfort cost. We consider both time-varying energy charge and demand charge caused by peak electrical power. With the help of CFD model, it allows us to deeply analyze thermal comfort and PMV. As results, we search for a possible set of the set-point temperature. In addition, we obtain an operating range for the volumetric flow rate which is connected to PMV calculation. In an MPC layer, the MPC tracks the optimal set-point from the SC layer and makes sure that the constraints are satisfied. The cost function of the MPC is composed of tracking error and control effort. Furthermore, we have done experiments

on various weather conditions to show that our proposed control design successfully achieves our control objectives.

1.2 Objective

The objective of this research aims to design a supervisory MPC for a building HVAC system that concerns thermal comfort and minimizes electricity consumption.

1.3 Scope

In this thesis,

- we consider a building consisting of a single zone equipped with one HVAC system which is modelled by energy and mass balance equations with lumped parameters. Controlled variables are zone temperature and zone humidity ratio. Manipulated variables are volumetric flow rate, heat exchanger electrical power, and removed moisture. Interaction between volumetric flow rate and air velocity inside the room is represented by computational-fluid-dynamic model.
- we design an MPC which its objective functions are to minimize an electricity consumption and regulate zone thermal comfort. To evaluate the zone thermal comfort, we regard the PMV which is connected to zone temperature, zone humidity, and air velocity.
- we simulate a data acquisition system to obtain disturbances data which are outside air temperature, outside air humidity ratio, heat load inside the zone, and humidity load inside the zone.
- we focus on solving the supervisory MPC problem numerically.

1.4 Contributions

In this thesis, we point our contribution as below.

- We formulate a novel design of supervisory MPC and show that it can be applied in

practice. In the SC layer, we deliberate on the formulation including the analysis of the response, the coostraint, and the trade-off between control objectives.

- We apply the proposed control design to the complex building HVAC system and proposed the MPC design that ensure regulation of temperature, humidity, and thermal comfort. In addition, our design successfully shaves peak-load and yields a better results of reference tracking.

- We show that the optimal set-point obtained from the proposed control design is able to reduce total operating cost and give the minimum thermal comfort deviation. Furthermore, the proposed control design smooths power profile and gives a superior output control.

- We rate computing time of the proposed control design to check feasibility of a real-time application. Our results reveal that the proposed control design adds only 10 ms to computing time of a standalone MPC.

1.5 Organization of Thesis

The organization of this thesis is as follows. A mathematical model of the HVAC system is given in Chapter 2 consisting of a dynamical model of indoor air temperature and humidity and a CFD model of indoor air speed. Chapter 3 provides a formulation of a supervisory MPC problem including an idea of the set-point design. For the SC layer, we search for an optimal set-point temperature with the help of disturbances data and transfer functions. Consequently, the MPC layer provides optimal control inputs to serve reference tracking and control effort. Numerical examples including patterns of optimal set-points, trade-off among objectives, and the results from the MPC are illustrated in Chapter 4. Lastly, conclusions and directions for future research are given in Chapter 5.

CHAPTER II

MATHEMATICAL MODEL OF ZONE AND HVAC SYSTEM

In this thesis, we consider a complex HVAC system that consider both thermal system and humidity system. List of related parameters and variables are illustrated in Table 2.1. As illustrated in Figure 2.1, the model is adapted from [21] and consists of four components, namely, a zone, a duct and mixing box and a heat exchanger, and a dehumidifier.

Table 2.1: Nomenclature of the HVAC system.

Notation	Definition	Value
A_{R}	Surface area of roof (m^2)	24
A_{W1}	Surface area of XZ wall (m^2)	15
A_{W2}	Surface area of YZ wall (m^2)	10
C_{D}	Heat capacity of duct wall (kJ/K)	0.42
C_{R}	Heat capacity of roof (kJ/K)	53.3
C_{W1}	Heat capacity of XZ wall (kJ/K)	46.7
C_{W2}	Heat capacity of YZ wall (kJ/K)	40.0
COP	Coefficient of performance	4
c_{pa}	Specific heat capacity of air ($\mathrm{kJ/kg \cdot K}$)	1.01
$d_{\mathrm{x}}, d_{\mathrm{y}}, d_{\mathrm{z}}$	Zone length, width, height (m)	$6, 4, 2.5$
f	Volumetric flow rate (m^3/s)	
h	Removed moisture in dehumidifier (kg/s)	
h_{fg}	Enthalpy of evaporation (kJ/kg)	2257
$L_{\mathrm{x}}, L_{\mathrm{y}}, L_{\mathrm{z}}$	Living space length, width, height (m)	$3, 2, 1.7$
M_{D}	Mass of duct (kg)	12.8
N_{oc}	The number of occupants	

P	Heat exchanger electrical power (W)	
Q_{L}	Heat load inside zone (W)	
Notation	Definition	Value
T_{D}	Air temperature inside duct (°C)	
T_{DH}	Air temperature inside dehumidifier (°C)	
T_{HE}	Air temperature inside heat exchanger (°C)	
T_{o}	Outside air temperature (°C)	
T_{R}	Temperature of roof (°C)	
T_{W1}	Temperature of XZ wall (°C)	
T_{W2}	Air temperature of YZ wall (°C)	
T_{Z}	Air temperature inside zone (°C)	
U_{Di}	Inner heat transfer coefficient of duct ($\mathrm{W/m^2K}$)	8.3
U_{Do}	Outer heat transfer coefficient of duct ($\mathrm{W/m^2K}$)	16.6
U_{R}	Heat transfer coefficient of roof ($\mathrm{W/m^2K}$)	5
U_{W1}	Heat transfer coefficient of XZ wall ($\mathrm{W/m^2K}$)	10
U_{W2}	Heat transfer coefficient of YZ wall ($\mathrm{W/m^2K}$)	10
$(UA)_{\mathrm{DH}}$	Overall heat transfer coefficient of dehumidifier (W/K)	27.5
$(UA)_{\mathrm{HE}}$	Overall heat transfer coefficient of heat exchanger (W/K)	60
V_{DH}	Volume of dehumidifier ($\mathrm{m^3}$)	2.16
V_{HE}	Volume of heat exchanger ($\mathrm{m^3}$)	4.32
V_{Z}	Volume of zone ($\mathrm{m^3}$)	75
ρ_{a}	Air density at 25 °C ($\mathrm{kg/m^3}$)	1.184
μ_{a}	Air viscosity at 25 °C ($\mu\mathrm{g \cdot s/m}$)	0.185
ω_{D}	Air humidity ratio inside duct (kg/kg)	
ω_{DH}	Air humidity ratio inside dehumidifier (kg/kg)	
ω_{HE}	Air humidity ratio inside heat exchanger (kg/kg)	
ω_{o}	Outside air humidity ratio (kg/kg)	
ω_{L}	Humidity load inside zone (kg/s)	
ω_{Z}	Air humidity ratio inside zone (kg/kg)	

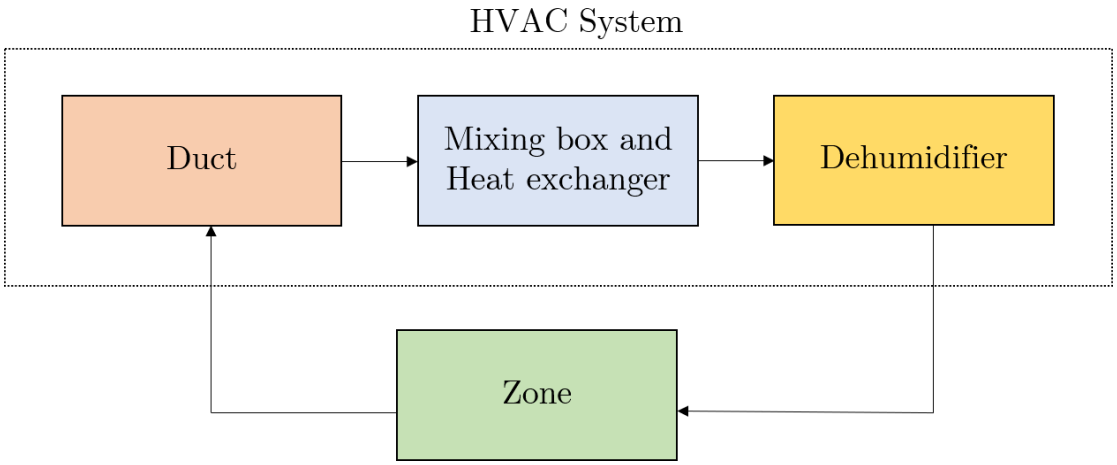

Figure 2.1: Considered HVAC system.

Based on Thailand weather condition, outside air temperature is commonly higher than zone temperature. Therefore, we can consider only air-conditioning mode of the HVAC system.

Firstly, we assume well-mixed air and lumped parameters properties. Thus, we can simply explain thermal system and humidity system using ordinary differential equations derived from energy and mass balance equations. To demonstrate an interaction between thermal system and humidity system, we use an idea of enthalpy of evaporation mentioned in [22]. Unlike [21], we treat volumetric flow rate as one of the control inputs. Therefore, the model is nonlinear. Control inputs of the HVAC system are volumetric flow rate (f), heat exchanger electrical power (P), and removed moisture (h).

2.1 Zone model

We focus on a single zone building shown in Figure 2.2 with the dimension of $d_{\mathrm{x}} \times d_{\mathrm{y}} \times d_{\mathrm{z}}$. The blue zone shows an occupied space for users and has a dimension of $L_{\mathrm{x}} \times L_{\mathrm{y}} \times L_{\mathrm{z}}$. The inlet air comes from the dehumidifier and has volumetric flow rate equal to f.

Let us define T_{Z}, T_{R} T_{W1}, T_{W2}, T_{DH}, ω_{Z} and ω_{DH} as zone temperature, roof temperature, XZ wall temperature, YZ wall temperature, dehumidifier air temperature, zone humidity ratio, and dehumidifier air humidity ratio, orderly.

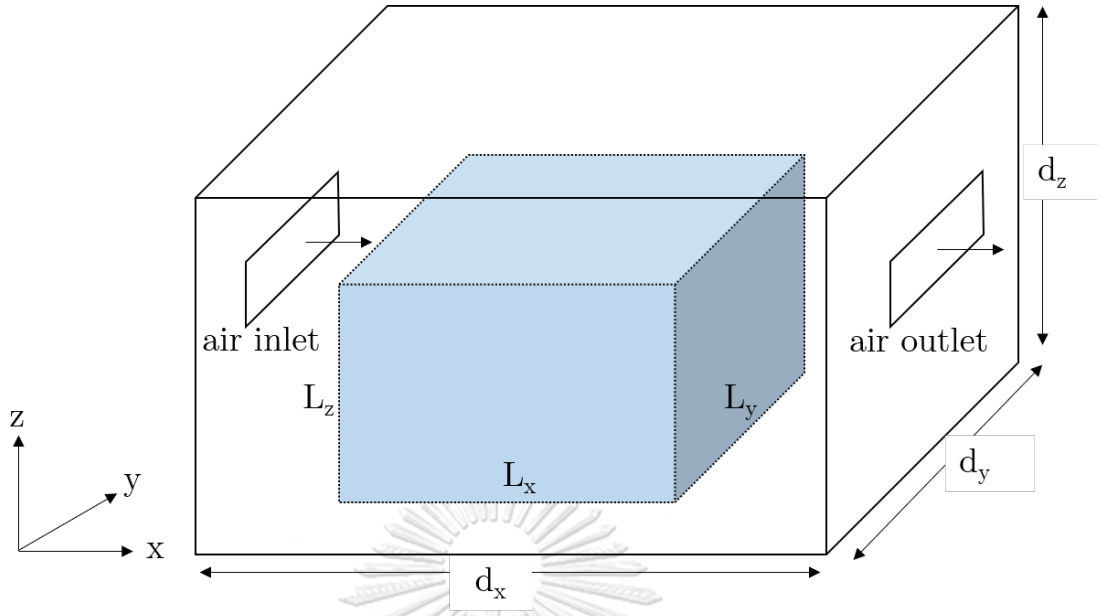

Figure 2.2: Zone model.

We can derive ordinary differential equation of the zone model as follows.

$$\begin{aligned} C_{\mathrm{a}}\rho_{\mathrm{a}}V_{\mathrm{Z}}\dot{T}_{\mathrm{Z}} &= U_{\mathrm{R}}A_{\mathrm{R}}(T_{\mathrm{R}}-T_{\mathrm{Z}}) + 2U_{\mathrm{W1}}A_{\mathrm{W1}}(T_{\mathrm{W1}}-T_{\mathrm{Z}}) \\ &\quad + 2U_{\mathrm{W2}}A_{\mathrm{W2}}(T_{\mathrm{W2}}-T_{\mathrm{Z}}) + \rho_{\mathrm{a}}fC_{\mathrm{a}}(T_{\mathrm{DH}}-T_{\mathrm{Z}}) \\ &\quad + Q_{\mathrm{L}} - h_{\mathrm{fg}}\rho_{\mathrm{a}}f(\omega_{\mathrm{DH}}-\omega_{\mathrm{Z}}) - h_{\mathrm{fg}}\omega_{\mathrm{L}}, \end{aligned} \tag{2.1}$$

$$C_{\mathrm{R}}\dot{T}_{\mathrm{R}} = U_{\mathrm{R}}A_{\mathrm{R}}(T_o-T_{\mathrm{R}}) + U_{\mathrm{R}}A_{\mathrm{R}}(T_{\mathrm{Z}}-T_{\mathrm{R}}), \tag{2.2}$$

$$\begin{aligned} C_{\mathrm{W1}}\dot{T}_{\mathrm{W1}} &= U_{\mathrm{W1}}A_{\mathrm{W1}}(T_o-T_{\mathrm{W1}}) \\ &\quad + U_{\mathrm{W1}}A_{\mathrm{W1}}(T_{\mathrm{Z}}-T_{\mathrm{W1}}), \end{aligned} \tag{2.3}$$

$$\begin{aligned} C_{\mathrm{W2}}\dot{T}_{\mathrm{W2}} &= U_{\mathrm{W2}}A_{\mathrm{W2}}(T_o-T_{\mathrm{W2}}) \\ &\quad + U_{\mathrm{W2}}A_{\mathrm{W2}}(T_{\mathrm{Z}}-T_{\mathrm{W2}}), \end{aligned} \tag{2.4}$$

$$V_{\mathrm{Z}}\dot{\omega}_{\mathrm{Z}} = f(\omega_{\mathrm{DH}}-\omega_{\mathrm{Z}}) + \frac{\omega_{\mathrm{L}}}{\rho_a}, \tag{2.5}$$

where Q_{L} and ω_{L} are internal heat load and humidity load, respectively. T_o is outside air temperature.

In general, air velocity is closely connected to volumetric flow rate or air change

per hour inside the room. To analyze an air velocity profile, we then construct a CFD model using the Navier-Strokes equation [23] for our zone model.

Under an assumption that the zone air is an incompressible Newtonian fluid, the Navier-Strokes equation for air velocity is written as

$$\rho_a \nabla v_a = -\nabla \mathcal{P} + \mu_a \nabla^2 v_a + \rho g \tag{2.6}$$

where ρ_a is air density, v_a is air velocity, $\mathcal{P}$ is air pressure, μ_a is air viscosity, and g is the standard gravity. $\nabla(\cdot)$ represents a first-order differential operator and $\nabla^2(\cdot)$ represents a second-order differential operator whereas axes of derivatives are regarding to Figure 2.2.

We can see that Equation Equation (2.6) is clearly a partial differential equation. To solve this equation, we choose Finite-difference method (FDM) which divides a space into a grid. Each node of the grid has different velocities, thus we regard air root-mean-squares (RMS) velocity ($v_{\text{a,rms}}$) as a representative for air velocity inside the occupied area.

$$v_{\text{a,rms}} = \sqrt{\frac{\sum_{i=1}^{N_{\text{node}}} v_{\text{a}}^2(x_i, y_i, z_i)}{N_{\text{node}}}}, \tag{2.7}$$

where i is an index of the node and N_{node} is the number of nodes inside the living space.

Since a relationship between air change per hour and volumetric flow rate is linear by its definition, there is a recommendation that affine approximation can be applied to approximate air velocity as a function of volumetric flow rate. In addition, we notice that volumetric flow rate also affects air RMS velocity. Thus, we approximate air RMS velocity inside the occupied zone by

$$\bar{v}_{\text{a,rms}}(f) = m_v f + b_v, \tag{2.8}$$

where $\bar{v}_{\text{a,rms}}$ is an approximate RMS air velocity, m_v and b_v are proper coefficients.

2.2 HVAC System

2.2.1 Duct

Duct is a component that returns air to the other components of the HVAC system. We suppose that the duct is lossless, which means there is no pressure loss. As results, humidity ratio inside the duct is equal to that of zone ($\omega_{\mathrm{D}} = \omega_{\mathrm{Z}}$). We explain the dynamic equation of the thermal system as follows

$$M_{\mathrm{D}} C_{\mathrm{D}} \dot{T}_{\mathrm{D}} = \frac{(U_{\mathrm{Di}} + U_{\mathrm{Do}})}{U_{\mathrm{Di}}} f \rho_{\mathrm{a}} C_{\mathrm{a}} (T_{\mathrm{Z}} - T_{\mathrm{D}}), \tag{2.9}$$

2.2.2 Mixing Box and Heat Exchanger

A mixing box and a heat exchanger is an equipment for a conversion between electrical power (P) and heat. Firstly, we assume that power conversion rate, which is described by coefficient of performance (COP), is a constant gain. Then, we specify mixing ratio between air from the duct and outside air is equal to 0.75:0.25.

To describe dynamic equation of the mixing box and the heat exchanger, we define T_{HE} as an air temperature inside the mixing box and the heat exchanger and define ω_{HE} as an air humidity ratio inside the mixing box and the heat exchanger. Thus, dynamic equation of the mixing box and the heat exchanger can be expressed as

$$\begin{aligned} C_{\mathrm{a}} \rho_{\mathrm{a}} V_{\mathrm{HE}} \dot{T}_{\mathrm{HE}} = {} & f C_{\mathrm{a}} \rho_{\mathrm{a}} (0.25 T_{\mathrm{o}} + 0.75 T_{\mathrm{D}} - T_{\mathrm{HE}}) \\ & + (UA)_{\mathrm{HE}} (T_{\mathrm{o}} - T_{\mathrm{HE}}) - \mathrm{COP} \cdot P \\ & - f \frac{h_{\mathrm{fg}}}{\rho_{\mathrm{a}}} (0.25 \omega_{\mathrm{o}} + 0.75 \omega_{\mathrm{Z}} - \omega_{\mathrm{HE}}), \end{aligned} \tag{2.10}$$

$$V_{\mathrm{HE}} \dot{\omega}_{\mathrm{HE}} = f (0.25 \omega_{\mathrm{o}} + 0.75 \omega_{\mathrm{Z}} - \omega_{\mathrm{HE}}), \tag{2.11}$$

where ω_{o} is outside humidity ratio.

2.2.3 Dehumidifier

A dehumidifier is a moisture control equipment which aims to reduce humidity level from passthrough air. Let us define T_{DH} and ω_{DH} as an air temperature and an air humidity ratio inside the dehumidifier, orderly. We can derive dynamic equation of thermal system and humidity system of air inside the dehumidifier as

$$\begin{aligned} C_{\mathrm{a}}\rho_{\mathrm{a}}V_{\mathrm{DH}}\dot{T}_{\mathrm{DH}} &= fC_{\mathrm{a}}\rho_{\mathrm{a}}(T_{\mathrm{HE}} - T_{\mathrm{DH}}) \\ &\quad + (UA)_{\mathrm{DH}}(T_{\mathrm{o}} - T_{\mathrm{DH}}) \\ &\quad - f\frac{h_{\mathrm{fg}}}{\rho_{\mathrm{a}}}(\omega_{\mathrm{HE}} - \omega_{\mathrm{DH}}) - h_{\mathrm{fg}}h, \end{aligned} \tag{2.12}$$

$$V_{\mathrm{DH}}\dot{\omega}_{\mathrm{DH}} = f(\omega_{\mathrm{HE}} - \omega_{\mathrm{DH}}) + \frac{h}{\rho_{\mathrm{a}}}, \tag{2.13}$$

where h denotes a removed moisture.

2.3 State-space Model

From above sections, it is clear that the HVAC model has a nonlinear characteristic. To eliminate nonlinearity, we employ linearization around an equilibrium point and discretize the model using zero-order hold method [27]. We select the equilibrium point by observation of steady state responses.

Firstly, we describe

$$\begin{aligned} x &= \begin{bmatrix} T_{\mathrm{Z}} & T_{\mathrm{R}} & T_{\mathrm{W1}} & T_{\mathrm{W2}} & T_{\mathrm{D}} & T_{\mathrm{HE}} & T_{\mathrm{DH}} & \omega_{\mathrm{Z}} & \omega_{\mathrm{HE}} & \omega_{\mathrm{DH}} \end{bmatrix}^T, \\ u &= \begin{bmatrix} f & P & h \end{bmatrix}^T, \\ v &= \begin{bmatrix} T_{\mathrm{o}} & Q_{\mathrm{L}} & \omega_{\mathrm{o}} & \omega_{\mathrm{L}} \end{bmatrix}^T, \\ y &= \begin{bmatrix} T_{\mathrm{Z}} & \omega_{\mathrm{Z}} \end{bmatrix}^T, \end{aligned}$$

where x is a state vector, u is a control input vector, v is a disturbance vector, and y is an output vector.

Next, we consider perturbation form of these vectors denoted as $\mathbf{x}$, $\mathbf{u}$, $\mathbf{v}$, and $\mathbf{y}$,

respectively. We then obtain

$$\mathbf{x} = x - \bar{x}, \mathbf{u} = u - \bar{u}, \mathbf{v} = v - \bar{v}, \mathbf{y} = y - \bar{y}.$$

We specify equilibrium point of volumetric flow rate and removed moisture to be 50 % of its operating range. For heat exchanger electrical power, we search for amount of power that gives zone temperature is around 25 °C. For the disturbances, we simply choose its average value. Consequently, equilibrium state $\bar{x}$ and equilibrium output $\bar{y}$ are obtained from solving steady state condition. Thus, we can write discrete-time linearized state-space model as

$$\begin{aligned} \mathbf{x}[k+1] &= \mathbf{A}\mathbf{x}[k] + \mathbf{B_u}\mathbf{u}[k] + \mathbf{B_v}\mathbf{v}[k], \\ \mathbf{y}[k] &= \mathbf{C}\mathbf{x}[k], \end{aligned} \tag{2.14}$$

where $\mathbf{A} \in \mathbb{R}^{n_x \times n_x}$, $\mathbf{B_u} \in \mathbb{R}^{n_x \times n_u}$, $\mathbf{B_v} \in \mathbb{R}^{n_x \times n_v}$, and $\mathbf{C} \in \mathbb{R}^{n_y \times n_x}$ are system matrices.

2.4 Summary

In this chapter, we introduce the mathematical model of the zone and the HVAC system. We apply an idea of enthalpy of evaporation to realize an interaction between air temperature and humidity. Moreover, we acknowledge that once volumetric flow rate is a control input, air velocities at each position of the zone are varied. We suggest a linear approximation of air RMS velocity as a linear function of the volumetric flow rate. Therefore, we apply the Navier-Strokes equation to develop a CFD model for an air inside the zone. Lastly, we observe that the dynamical model has nonlinear elements. To eliminate the nonlinearity of the model, we simply linearize the model with the zero-order hold method.

CHAPTER III

SUPERVISORY MODEL PREDICTIVE CONTROL

3.1 Predicted Mean Vote (PMV)

To score thermal comfort of occupants, we consider Predicted Mean Vote (PMV) which is accepted as a thermal comfort indicator in ASHRAE55 [12].

Value of PMV implies score of occupants feeling about their comfort. For example, plus PMV means users feel hot. On the other hand, minus PMV denotes users feel cool. Zero PMV level implies users has neutral feeling about their comfort satisfaction and implies ideal comfort. We summarize interpretation of thermal comfort from PMV in Table 3.1.

Table 3.1: PMV value and comfort satisfaction [12].

PMV value	**Thermal comfort satisfaction**
+3	hot
+2	warm
+1	slightly warm
0	neutral
-1	slightly cool
-2	cool
-3	cold

According to [12], an admittable range of PMV is in a range of -0.5 to +0.5. Calculation of PMV involves zone temperature, zone humidity, air velocity as well as users' parameters. Equation of PMV calculation can be expressed as the following equations.

$$
\begin{aligned}
\mathrm{PMV} &= 0.303 \cdot \exp(-0.036 \cdot M + 0.028)L \\
L &= (M - W) \\
&\quad - 3.05 \cdot 10^{-3}(5733 - 6.99(M - W) - p_{\mathrm{a}}) \\
&\quad - 0.42((M - W) - 58.15) \\
&\quad - 1.7 \cdot 10^{-5} M(5867 - p_{\mathrm{a}}) - 0.0014M(34 - T_{\mathrm{Z}}) \\
&\quad - 3.96 \cdot 10^{-8} f_{cl}(K_{tcl} - K_{tr}) - f_{cl} h_c (T_{cl} - T_{\mathrm{Z}}) \\
T_{cl} &= 35.7 - 0.028(M - W) \\
&\quad - I_{cl}(f_{cl} h_c (T_{cl} - T_{\mathrm{Z}}) \\
&\quad + 3.96 \cdot 10^{-8} f_{cl}(K_{tcl} - K_{tr})) \\
K_{tcl} &= (T_{cl} + 273.15)^4 \\
K_{tr} &= (T_{\mathrm{Z}} + 273.15)^4 \\
p_a &= 6.1094 \cdot \mathrm{RH} \cdot \exp(\frac{17.625 \cdot T_{\mathrm{Z}}}{T_{\mathrm{Z}} + 243.04}) \\
h_c &= \begin{cases} 2.38 \cdot |T_{cl} - T_{\mathrm{Z}}|^{0.25}, & \text{if } 2.38|T_{cl} - T_{\mathrm{Z}}|^{0.25} \geq 12.1\sqrt{v_a}, \\ 12.1\sqrt{v_a}, & \text{otherwise,} \end{cases} \\
f_{cl} &= \begin{cases} 1.00 + 1.290 I_{\mathrm{cl}}, & \text{if } I_{\mathrm{cl}} \leq 0.078 \\ 1.05 + 0.645 I_{\mathrm{cl}}, & \text{otherwise.} \end{cases}
\end{aligned}
\tag{3.1}
$$

T_{cl} is clothing surface temperature (°C), p_a is water vapor partial pressure (Pa), h_c is a convective heat transfer coefficient (W/m^{2}K), and f_{cl} is a clothing surface area factor. The other variables are as follows. M is a metabolic rate (W/m^2), W is excreted work (W/m^2), I_{cl} is a clothing index, v_{a} is air velocity (m/s), T_{rm} is mean radiant temperature (°C), and RH is relative humidity.

To simplify the calculation, the following assumptions are made. Firstly, due to complication of real-world measuring, we suppose that mean radiant temperature is equal to zone temperature. Secondly, we simplify relative humidity so that the saturation humidity ratio is supposed to be constant. Thirdly, we presume that there is no heat

source inside the zone. Therefore, excreted work is equal to zero. More details about metabolic rate and clothing material can be found in [12]. Next, we then apply Equation (2.8) to approximate air RMS velocity regarding to volumetric flow rate.

We acknowledge that change of PMV is caused by change of zone temperature as well as change of air velocity. On the other hand, we observe that PMV has a low sensitivity to change of zone humidity. Therefore, we choose zone temperature and air velocity to be main consideration which affects PMV.

3.2 Recommended Operating Range of Volumetric Flow Rate

Due to relationship in Equation (2.14), magnitude of volumetric flow rate is obviously related to that of heat exchanger electrical power. To reduce electricity peak demand of the HVAC system, we suggest a practical selection of volumetric flow rate due to various types of weather conditions. We select major disturbances impacted on control performance, which are outside temperature and outside humidity ratio, as independent variables whereas volumetric flow rate becomes a dependent variable. Next, we applied the average of outside temperature ($\overline{T_{\mathrm{o}}}$) and the average of outside RH ($\overline{\mathrm{RH_o}}$) to classify weather conditions.

Let us define $T_{\mathrm{o,h}}$, $T_{\mathrm{o,l}}$, $\mathrm{RH_{o,h}}$, $\mathrm{RH_{o,l}}$ as high threshold of average outside temperature low threshold of average outside temperature, high threshold of average outside RH, and low threshold of average outside RH, respectively. Therefore, we have nine weather conditions. After that, we explore a proper setting for volumetric flow rate to create a projection from weather conditions to volumetric flow rate which is illustrated in Table 3.2.

Table 3.2 represents general idea of volumetric flow rate selection based on our HVAC system. When outside temperature is high, we suggest using higher volumetric flow rate than nominal operation to increase heat exchanging rate. As results, electrical power consumed by heat exchanger can be reduced while zone temperature is controlled. For the sake of understanding, we give some illustrative scenarios as follows.

Table 3.2: Recommended operating range of volumetric flow rate regarding to weather conditions.

	Average humidity		
Average temp.	$\overline{\mathrm{RH}}_{\mathrm{o}} > \mathrm{RH}_{\mathrm{o,h}}$	$\mathrm{RH}_{\mathrm{o,l}} < \overline{\mathrm{RH}}_{\mathrm{o}} < \mathrm{RH}_{\mathrm{o,h}}$	$\overline{\mathrm{RH}}_{\mathrm{o}} < \mathrm{RH}_{\mathrm{o,l}}$
$\overline{T}_{\mathrm{o}} > T_{\mathrm{o,h}}$	**Medium** to **High**	**High**	**High**
$T_{\mathrm{o,l}} < \overline{T}_{\mathrm{o}} < T_{\mathrm{o,h}}$	**Medium** to **High**	**Medium** to **High**	**Medium** to **High**
$\overline{T}_{\mathrm{o}} < T_{\mathrm{o,l}}$	**Low** to **High**	**Medium**to **High**	**Medium** to **High**

In summer season, outside temperature is higher than $T_{\mathrm{o,h}}$ whearas outside humidity is in moderate level. Using Table 3.2, we recommend using **High** for the operating range of volumetric flow rate.

In rainy season, outside temperature is higher than $T_{\mathrm{o,h}}$ whearas outside humidity is very high. We suggest that the operating range of volumetric flow rate should be set in a range of **Medium** to **High**.

In winter season, outside temperature is lower than $T_{\mathrm{o,l}}$ whereas outside humidity is in moderate level. Thus, **Medium** to **High** is recommended for the operating range of volumetric flow rate.

3.3 Supervisory Control (SC)

To develop the SC design for the HVAC system, our work focuses on developing set-point design problem. The objectives of the SC layer is to compute optimal reference (**OptRef**). **OptRef** is constructed by using historical disturbances and thermal comfort boundary. Diagram of the SC layer is illustrated in Figure 3.1.

OptRef is composed of the optimal set-point temperature (T^{*}_{ref}). To design **OptRef**, we suppose that

Assumption 1 *The zone humidity ratio is constant at* ω_{ref}.

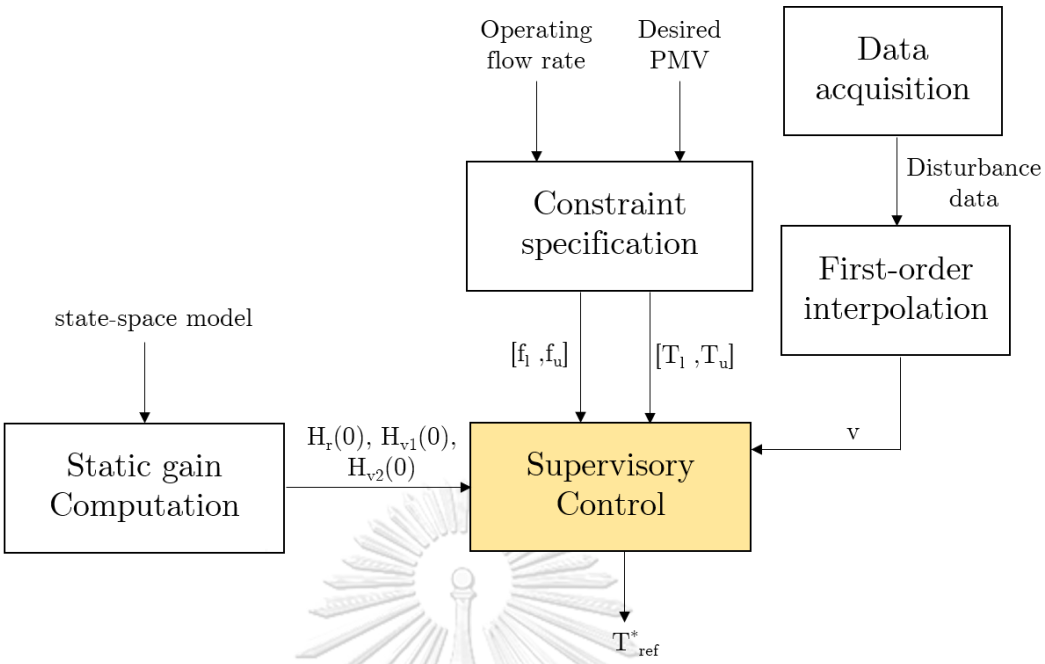

Figure 3.1: Block diagram of a supervisory control for the HVAC control system.

Assumption 2 *A transient response of the zone temperature is neglected.*

The first assumption means the humidity ratio is not included in the **OptRef** design. Once this assumption is hold, we note that zone temperature depends on electrical power (P), outside temperature (T_o), and heat load (Q_{L}).

The second assumption gives a reason that sampling time of the SC layer is longer than time constant of the HVAC model. This allows us to regard only steady state responses of the HVAC system.

We formulate **OptRef** design as a quadratic program. The cost function is composed of total operating cost (TOC) and thermal comfort cost (TCC). We specify a admittable boundary of PMV to derive constraints for **OptRef**.

Let us define T_{ref} as a set-point temperature. To formulate **OptRef**, we come up with a predesign HVAC control system whose block diagram is shown in Figure 3.2. Interaction among set-point temperature and the other variables are explained by transfer functions derived from Equation (2.14).

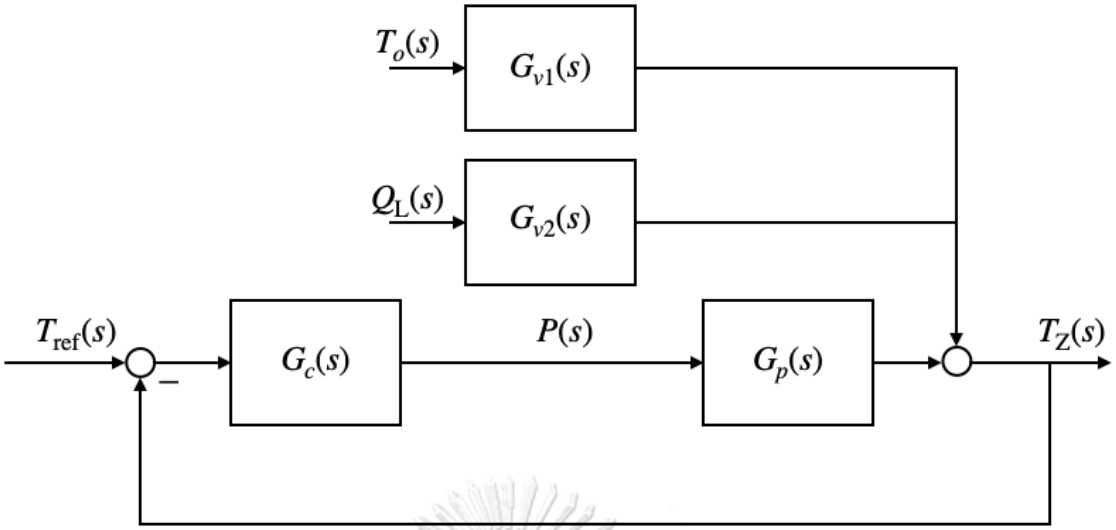

Figure 3.2: Block diagram of the predesign HVAC control system.

We denote $G_p(s)$ as a transfer function from the heat exchanger electrical power to zone temperature, $G_{v1}(s)$ as a transfer function from outside temperature to zone temperature, $G_{v2}(s)$ as a transfer function from heat load to zone temperature, and $G_c(s)$ as a controller transfer function. $G_c(s)$ is simply chosen to be a simple PID controller,

$$G_c(s) = K_P + \frac{K_I}{s} + K_D s.$$

due to consideration of steady state condition. Foe the choices of predesign controllers, we examine various settings of the PID controllers to evaluate characteristics of **OptRef**.

Next, let us define $H_r(s)$ as a closed-loop transfer function from the set-point temperature to the heat exchanger electrical power, $H_{v1}(s)$ as a closed-loop transfer function from the outside temperature to the heat exchanger electrical power, and $H_{v2}(s)$ as a closed-loop transfer function from the heat load to the heat exchanger electrical power. Thus, these transfer functions are expressed as

$$H_r(s) = \frac{P(s)}{T_{ref}(s)} = \frac{G_c(s)}{1 + G_c(s)G_p(s)},$$

$$H_{v1}(s) = \frac{P(s)}{T_o(s)} = \frac{G_{v1}(s)}{1 + G_c(s)G_p(s)},$$

$$H_{v2}(s) = \frac{P(s)}{Q_L(s)} = \frac{G_{v2}(s)}{1 + G_c(s)G_p(s)}.$$

Consequently, DC gains of these transfer functions, namely, $H_r(0)$, $H_{v1}(0)$, and $H_{v2}(0)$, can be derived. As results, equation of electrical power in the SC problem can be expressed in discrete time as

$$P[k] = H_r(0)T_{\text{ref}}[k] + H_{v1}(0)T_{\text{o}}[k] + H_{v2}(0)Q_{\text{L}}[k], \tag{3.2}$$

where k is a time index.

3.3.1 Total Operating Cost (TOC)

TOC can be divided into two components, energy charge (EC) and demand charge (DC). EC is computed by electrical energy consumed by the heat exchanger whereas DC regards peak-load. We can write equations of EC and Dc as

$$\text{EC} = \sum_{k=1}^{N_{\text{S}}} c_{\text{EC}}[k]P[k]t_{\text{s}}$$

$$\text{DC} = c_{\text{DC}} \max_{k=1,\ldots,N_{\text{S}}} \{P[k]\},$$

where N_{S} is the number of time interval. c_{EC} and c_{DC} are EC cost coefficient (THB/ kWh) and DC cost coefficient (THB/kW), orderly. Note that we consider c_{EC} as a time varying function based on modified time-of-use (TOU) tariff. t_{s} is sampling time of the SC layer. Therfore, TOC is expressed as

$$\text{TOC} = \text{EC} + \text{DC}. \tag{3.3}$$

Using Equation (3.2), Equation (3.3) can be written as a function of set-point temperature.

3.3.2 Thermal Comfort Cost (TCC)

Let us define T_0 as an ideal comfort temperature which gives PMV = 0. Next, we consider deviation of set-point temperature from T_0 (T_{ref}), where

$$\Delta T_{\text{ref}}[k] = T_{\text{ref}}[k]T_0.$$

TCC is defined by

$$\mathrm{TCC} = \sum_{k=1}^{N_\mathrm{S}} (T_\mathrm{ref}[k] - T_0)^2. \tag{3.4}$$

To determine a boundary of **OptRef**, we define a lower bound of set-point temperature (T_l) and a upper bound of set-point temperature (T_u). Therefore, the boundary of **OptRef** can be simply expressed as

$$T_\mathrm{l} \leq T_\mathrm{ref}[k] \leq T_\mathrm{u}. \tag{3.5}$$

We notice that T_0,T_l, and T_u are related to volumetric flow rates. In addition, we add an additional limit for set-point temperature with respect to outside air temperature

$$T_\mathrm{ref}[k] \leq T_\mathrm{o}[k]. \tag{3.6}$$

This constraint is important since our HVAC system aims to operate only in air-conditioning mode.

3.3.3 Formulation of SC Design Problem

We define $\mathrm{TOC}_\mathrm{min}$ as the minimum TOC when we use $T_\mathrm{ref} = T_\mathrm{u}$ with the HVAC system and define $\mathrm{TOC}_\mathrm{max}$ as the maximum TOC when $T_\mathrm{ref} = T_0$ is applied to the HVAC system. We introduce normalized TOC (J_TOC) where

$$J_\mathrm{TOC} = \frac{\mathrm{TOC} - \mathrm{TOC}_\mathrm{min}}{\mathrm{TOC}_\mathrm{max} - \mathrm{TOC}_\mathrm{min}}. \tag{3.7}$$

Likewise, J_TCC is defined as normalized TCC where

$$J_\mathrm{TCC} = \frac{\mathrm{TCC} - \mathrm{TCC}_\mathrm{min}}{\mathrm{TCC}_\mathrm{max} - \mathrm{TCC}_\mathrm{min}}. \tag{3.8}$$

$\mathrm{TCC}_\mathrm{min}$ is the minimum TCC (equal to zero when $T_\mathrm{ref} = T_0$) and $\mathrm{TCC}_\mathrm{max}$ is the maximum TCC which can be calculated by the following equation

$$\mathrm{TCC}_\mathrm{max} = \begin{cases} N_\mathrm{S} \cdot (T_\mathrm{l} - T_0)^2, & |T_\mathrm{l} - T_0| \geq |T_\mathrm{u} - T_0|, \\ N_\mathrm{S} \cdot (T_\mathrm{u} - T_0)^2, & \text{otherwise.} \end{cases}$$

Therefore, cost function of **OptRef** design problem can be written as

$$J_{\mathrm{S}} = (1-\alpha)J_{\mathrm{TOC}} + \alpha J_{\mathrm{TCC}}, \tag{3.9}$$

where α is an optimization weight which has a range of 0 to 1. Notice that the value of α implies the trade-off between TOC and TCC.

Thus, we can write **OptRef** design problem as

$$\begin{aligned} \underset{T_{\mathrm{ref}}}{\text{minimize}} \quad & J_{\mathrm{S}} \\ \text{s.t.} \quad & \text{(3.2), (3.5) and (3.6).} \end{aligned} \tag{3.10}$$

It is obvious that **OptRef** design problem is a quadratic program. Since the quadratic program has convex characteristic, we can efficiently solve the optimal solution T^*_{ref} with standard solvers. Once T^*_{ref} is obtained, we then perform up sampling using first-order interpolation and send it to the MPC.

3.4 Model Predictive Control

We suppose that all states are measurable. We can apply a standard MPC, shown in Figure 3.3, which its design procedure was stated in [14].

Firstly, the MPC recieved interpolated T^*_{ref} from the SC layer. We formulate the cost function of the MPC which is composed of reference tracking and control input minimizing. Let us define a set-point of the MPC (r)

$$r[k] = \begin{bmatrix} T^*_{\mathrm{ref}}[k] & \omega_{\mathrm{ref}}[k] \end{bmatrix}^T, \tag{3.11}$$

where k is a time index of the MPC layer.

Secondly, the MPC aims to calculate future control inputs based on current state $x[k]$. Due to receding horizon control principle, we only apply the first sequence of the future control inputs to the HVAC system.

We define state increment ($\boldsymbol{\Delta x}$) and input increment ($\boldsymbol{\Delta u}$) where

$$\boldsymbol{\Delta x} = x[k] - x[k-1], \ \boldsymbol{\Delta u} = u[k] - u[k-1].$$

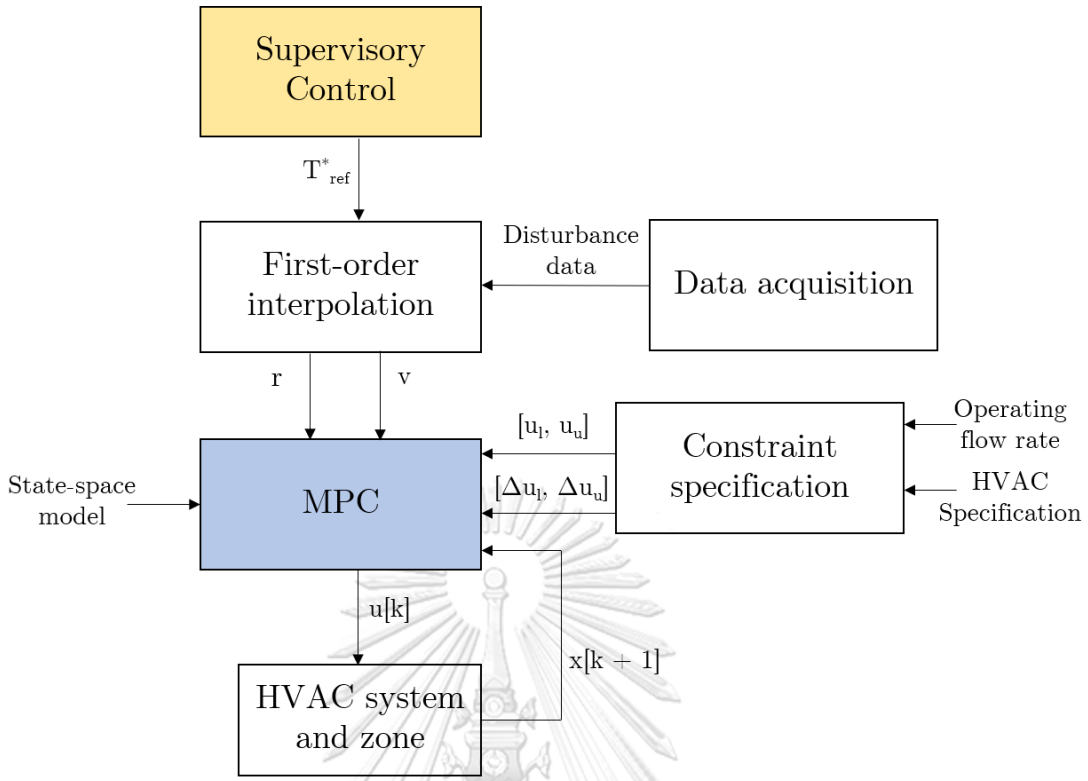

Figure 3.3: Block diagram of a model predictive control for the HVAC control system

Then, we can write an MPC input update equation as

$$\boldsymbol{u}[k] = \boldsymbol{u}[k-1] + \boldsymbol{\Delta u}[k \mid k].$$

$\boldsymbol{\Delta u}[k \mid k]$ is regarded as the input increment at time index k given state information at time index k. In the following section, we will use this equation to formulate the MPC optimization problem.

3.4.1 Constraint Specification

To realize the practical control design, we implement a constraint of control input ramp rate,

$$\Delta u_{\mathrm{l}} \leq \boldsymbol{\Delta u}[k+j \mid k] \leq \Delta u_{\mathrm{u}}, \forall j, \tag{3.12}$$

where $\Delta u_{\mathrm{l}} = \begin{bmatrix} \Delta f_{\mathrm{l}} & \Delta P_{\mathrm{l}} & \Delta h_{\mathrm{l}} \end{bmatrix}^T$, and $\Delta u_{\mathrm{u}} = \begin{bmatrix} \Delta f_{\mathrm{u}} & \Delta P_{\mathrm{u}} & \Delta h_{\mathrm{u}} \end{bmatrix}^T$ are lower and upper bounds of the input increments obtained from specifications of the HVAC system. Next, we incorporate a control input constraint,

$$u_{\mathrm{l}} \leq u[k] \leq u_{\mathrm{u}}, \tag{3.13}$$

$u_{\mathrm{l}} = \begin{bmatrix} f_{\mathrm{l}} & P_{\mathrm{l}} & h_{\mathrm{l}} \end{bmatrix}^T$, and $u_{\mathrm{u}} = \begin{bmatrix} f_{\mathrm{u}} & P_{\mathrm{u}} & h_{\mathrm{u}} \end{bmatrix}^T$ are lower and upper bounds of the control inputs.

Due to relationship between air velocity and volumetric flow rate, we note that PMV is greatly influence by air velocity as well as volumetric flow rate. Therefore, we search for a range of the volumetric flow rate that allows us to use **OptRef** without PMV violation.

An operating range of volumetric flow rate can be obtained from analysis of the PMV where f_{l} is selected to be greater than or equal to assigned volumetric flow rate from the SC layer whereas the HVAC specification describes f_{u}.

Next, a constraint for control inputs is calculated with respect to the equilibrium point. We subtract $\bar{u}$ from Equation (3.13) and obtain the following constraint

$$u_{\mathrm{l}} - \bar{u} \leq \boldsymbol{u}[k] \leq u_{\mathrm{u}} - \bar{u}, \forall k. \tag{3.14}$$

3.4.2 Formulation of MPC Design Problem

Firstly, we denote a future output vector ($\boldsymbol{Y}[k] \in \mathbb{R}^{N_P}$), future control input increment at time index k ($\boldsymbol{\Delta U}[k] \in \mathbb{R}^{N_C}$), and future reference signal ($\boldsymbol{r}[k]$). These vectors can be written as

$$\begin{aligned}
\boldsymbol{Y}[k] &= \begin{bmatrix} \boldsymbol{y}[k+1 \mid k] & \dots & \boldsymbol{y}[k+N_P \mid k] \end{bmatrix}^T, \\
\boldsymbol{\Delta U}[k] &= \begin{bmatrix} \boldsymbol{\Delta u}[k \mid k] & \dots & \boldsymbol{\Delta u}[k+N_C-1 \mid k] \end{bmatrix}^T, \\
\boldsymbol{r}[k] &= \begin{bmatrix} r[k+1] & \dots & r[k+N_P] \end{bmatrix}^T,
\end{aligned}$$

Where N_P is prediction horizon and N_C is control horizon. $\boldsymbol{y}[k+j \mid k]$ is future outputs at at time index $k+j$ given $x[k]$. Likewise, $\boldsymbol{\Delta u}[k+j \mid k]$ is future input increment at time index $k+j$ given $x[k]$.

To implement the dynamic equation of future response, we consider an augmented state space model,

$$\boldsymbol{Y}[k] = \boldsymbol{F}\boldsymbol{\Delta x}[k] + \boldsymbol{\Phi}\boldsymbol{\Delta U}[k], \tag{3.15}$$

where

$$\boldsymbol{F} = \begin{bmatrix} \boldsymbol{CA} & \boldsymbol{CA}^2 & \cdots & \boldsymbol{CA}^{N_P} \end{bmatrix}^T,$$

$$\boldsymbol{\Phi} = \begin{bmatrix} \boldsymbol{CB} & 0 & \cdots & 0 \\ \boldsymbol{CAB} & \boldsymbol{CB} & \cdots & 0 \\ \vdots & \vdots & \ddots & \vdots \\ \boldsymbol{CA}^{N_P-1}\boldsymbol{B} & \boldsymbol{CA}^{N_P-2}\boldsymbol{B} & \cdots & \boldsymbol{CA}^{N_P-N_C}\boldsymbol{B} \end{bmatrix}.$$

In the MPC cost function, we consider two objectives, namely, reference tracking and control effort. Therefore, we formulate The MPC cost function as

$$J_{\text{MPC}}[k] = \|Q^{1/2}(\boldsymbol{r}[k] - \boldsymbol{Y}[k])\|_2^2 + \|R^{1/2}\boldsymbol{\Delta U}[k]\|_2^2.$$

$Q \in \mathbb{R}^{(N_P \times n_y)\times(N_P \times n_y)}$ and $R \in \mathbb{R}^{(N_C \times n_u)\times(N_C \times n_u)}$ are optimization weight matrices.

Thus, we can write an MPC optimization problem as the following equation,

$$\begin{aligned} \underset{\boldsymbol{\Delta U}[k]}{\text{minimize}} \quad & J_{\text{MPC}}[k] \\ \text{s.t.} \quad & \text{(3.12), (3.14), and (3.15).} \end{aligned} \tag{3.16}$$

We note that we formulate MPC optimization problem as a quadratic program. Thus, we can ensure that the optimal control input is feasible and is global. In this thesis, we apply active-set SQP algorithm to solve the optimal solution. Since the quadratic program is convex, active-set SQP algorithm terminates within the finite iterations.

3.5 Summary

In this chapter, we present concepts and a formulation of the supervisory MPC problem. Firstly, we show an equation set of the PMV and an interpretation of users' thermal comfort. Secondly, we introduce a set-point temperature design on the SC layer based on disturbances data. With mentioned assumptions, we apply the transfer functions, TCC, and TOC to formulate the SC problem as a quadratic optimization problem. We apply the PMV to identify an allowable range of temperatures with respect

to the designed volumetric flow rate. Consequently, we formulate an MPC problem, received the optimal set-point from the SC layer, as a quadratic optimization problem with the reference tracking and control effort as its objective function. Lastly, we suggest a specification of constraints to confirm that PMV is in acceptable region.

CHAPTER IV

NUMERICAL EXAMPLES

4.1 Model of Zone and HVAC System

In our example, the zone is a square room directly contacted with outside air. The room has a function of administrative office with dimension of $d_{\mathrm{x}} \times d_{\mathrm{y}} \times d_{\mathrm{z}} = 6 \times 4 \times 2.5$ m^3. HVAC system parameters are given in Table 2.1. The dynamical model of HVAC model is nonlinear. We utilize the linearization around an equilibrium point which is obtained by choosing control inputs and disturbances then solving the steady state condition. An operating point of the volumetric flow rate and the removed moisture is chosen to be equal to 50% of the operating range, namely, 0.15 m^3/s and -0.0005 kg/s, respectively. For the electrical power of heat exchanger, we specify the operating point so that the equilibrium of zone temperature is about 25 °C. We choose the average values of disturbances for the equilibrium point analysis. Therefore, we obtain the operating point of control inputs, disturbances, and states as follows:

$$\bar{u} = \begin{bmatrix} 0.15 & 950 & -0.0005 \end{bmatrix}^T,$$
$$\bar{v} = \begin{bmatrix} 35 & 145.14 & 0.023 & -4.4 \times 10^{-5} \end{bmatrix}^T,$$

and

$$\bar{x} = [24.89 \quad 28.45 \quad 26.92 \quad 28.05 \quad 25.10$$
$$12.20 \quad 14.84 \quad 0.0121 \quad 0.0148 \quad 0.0118]^T.$$

Consequently, the linearized model of the HVAC system around the chosen operating point can be determined. Next, we specify $L_{\mathrm{x}} = 3$ m, $L_{\mathrm{y}} = 2$ m, and $L_{\mathrm{z}} = 1.7$ m for the living space. The area of the air inlet is equal to 0.25 m^2 and the area of the air outlet is equal to 0.5 m^2. The volumetric flow rate of the HVAC system is operating from 0.12 to 0.18 m^3/s. The air density and viscosity are given in Table 2.1. After analysis using

CFD model, we observe that a magnitude of the air velocity depends on the position of Y-axis and Z-axis. To solve (2.6) by FDM, we consider 151×151 nodes with a grid size of 0.0267×0.0167 m^2. With this setting, the zone contains 22801 nodes and the living space contains 7752 nodes. We calculate the RMS air velocity for $N_{\text{node}} = 7752$ nodes using (2.7). Then, we approximate the air velocity as an affine function of volumetric flow rate via (2.6)–(2.8). We obtain $m_v = 2.4357$ and $b_v = -0.1754$. That is

$$\bar{v}_{\text{a,rms}}(f) = 2.4357f - 0.1754,$$

Figure 4.1 depicts the actual data and the fitting result of $R^2 = 0.9898$.

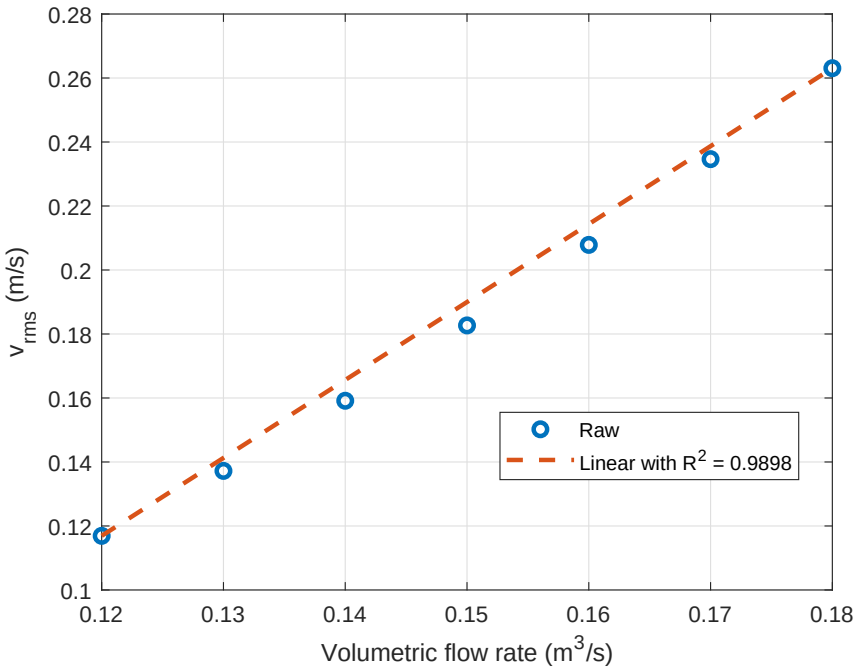

Figure 4.1: Affine approximation of the RMS air velocity inside the living space.

4.2 Analysis of PMV

We analyze the effects of various factors on the PMV. First, we specify the saturation humidity ratio = 0.022 kg/kg which is a standard value at 25 °C. For the fixed parameters, we choose $M = 70$ and $I_{\text{cl}} = 0.67$ clo. In the example, we choose an equilibrium point to be RH = 55%, $T_{\text{Z}} = 25$ °C, and $v_a = 0.19$ m/s connected to $f = 0.15$ m^3/s for the operating condition of the HVAC system. Then, we calculate the PMV when

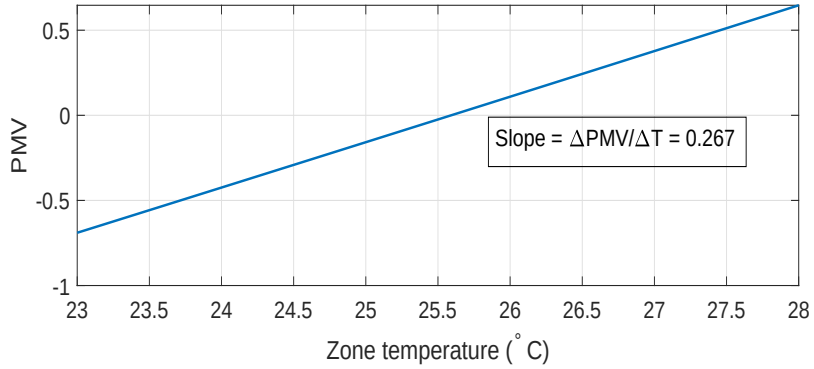

(a)

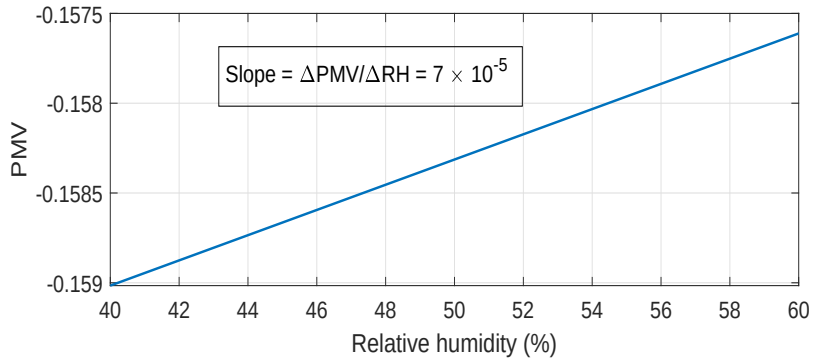

(b)

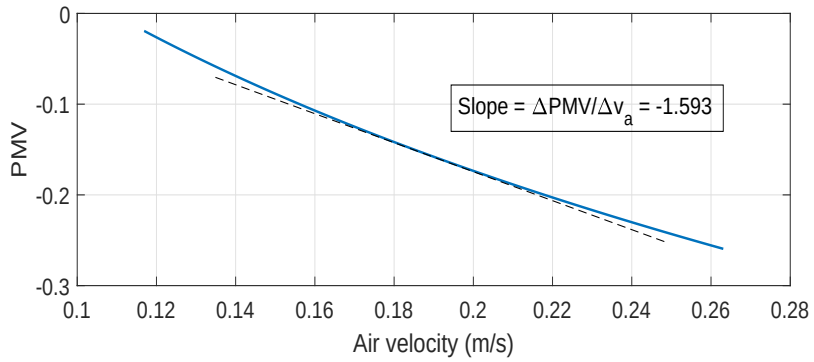

(c)

Figure 4.2: PMV with respect to the zone temperature, the zone relative humidity, and the air velocity around the equilibrium point where (a) The PMV versus the zone temperature (b) The PMV versus the zone relative humidity (c) The PMV versus the air velocity.

varying the zone temperature, the zone relative humidity, and the air velocity. The PMV plots are shown in Figure 4.2.

From the results, we clearly see that the zone temperature and the air velocity have strong effects on the PMV with the slopes 0.2673/°C and $-1.593/(\mathrm{m/s})$), respectively. However, the zone relative humidity has a weak effect on the PMV with a slope of 7×10^{-5}. From sensitivity analysis, it supports our assumption that the relative humidity can be neglected from the SC design problem.

Next, we examine the ideal comfort temperature (T_0), the lower bound (T_l) and the upper bound (T_u) of the set-point zone temperature where the volumetric flow rate is operating within the specified range. In this numerical example, T_l is connected to PMV $= -0.2$ and T_u is connected to PMV $= 0.5$.

Table 4.1: Ideal comfort temperature, lower and upper bound of the set-point zone temperature corresponding to the volumetric flow rates.

Volumetric flow rate (m^3/s)	T_0(°C)	T_l(°C)	T_u(°C)
0.12	25.08	24.28	27.06
0.13	25.28	24.50	27.22
0.14	25.45	24.68	27.35
0.15	25.59	24.84	27.46
0.16	25.72	24.98	27.55
0.17	25.83	25.10	27.64
0.18	25.93	25.21	27.71

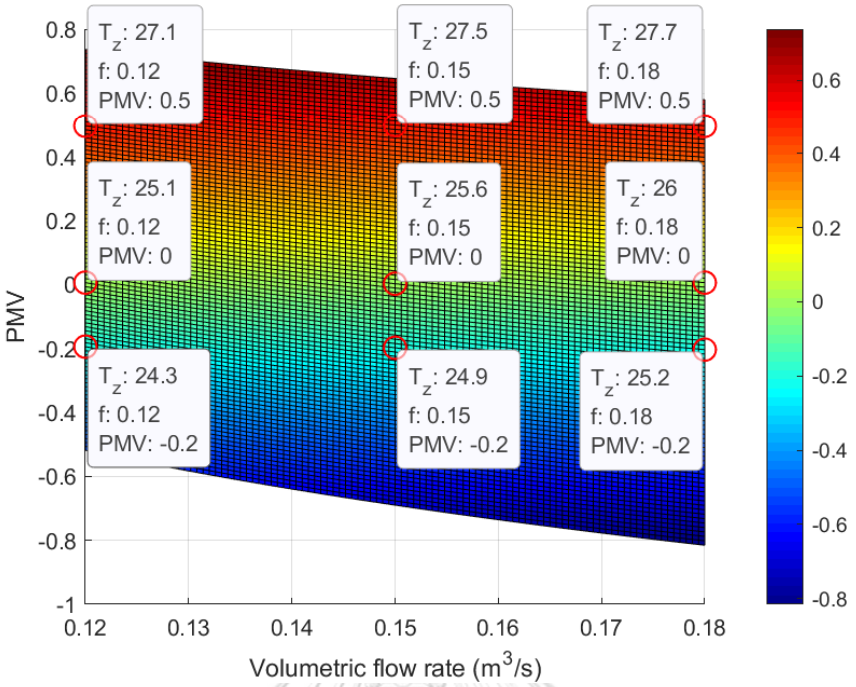

Figure 4.3: Region of the zone temperature and the volumetric flow rate while the PMV is in a range of -0.2 to 0.5.

In Table 4.1, we observe that an increase of the volumetric flow rates leads to an increase of the T_0, T_l, and T_u. Since T_0, T_l, and T_u are corresponding to the PMV, this implies that increasing the volumetric flow rate enables the higher set-point of zone temperature while the PMV is maintained in an acceptable level.

Next, we consider the region of zone temperature and volumetric flow rate corresponding to the PMV shown in Figure 4.3. We observe that the range of volumetric flow rate is corresponding to the range of PMV. In particular, we can specify a proper constraint of the volumetric flow rate to ensure the PMV well regulated.

4.3 Experiment Setup

4.3.1 Supervisory Control

We select the sampling time of the SC design (t_s) to be 15 minutes and the simulation duration is 9 hours. Therefore, $N_\mathrm{S} = 37$ samples including the initial point.

To calculate the TOC, we use the modified TOU tariff shown in Figure 4.4.

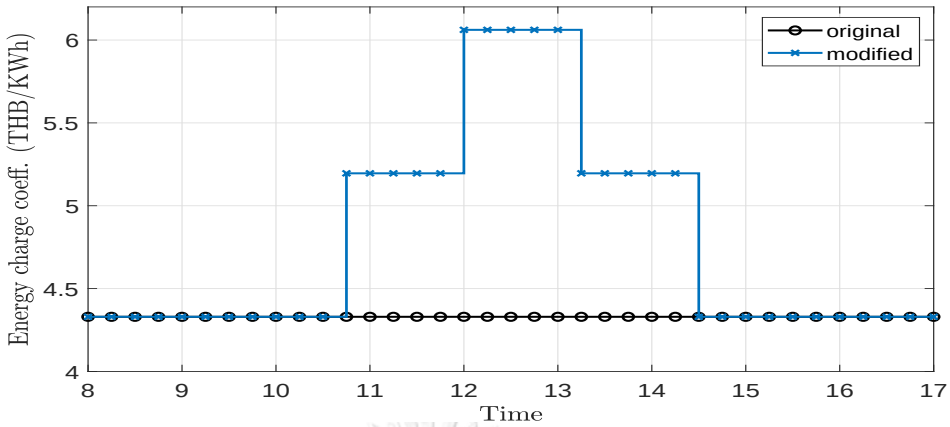

Figure 4.4: Original TOU tariff [30] and modified TOU tariff.

The reason to modify the TOU tariff is that it penalizes the energy cost during the time when the peak load occurs. We use $c_{\mathrm{DC}} = 210$ THB/kW and c_{EC} in THB/kWh is represented by a stair function. We specify $\omega_{\mathrm{ref}} = 0.012$ kg/kg which is connected to RH $= 54.5\%$. The lower bound and the upper bound of the PMV are chosen to be -0.2 and 0.5, respectively.

4.3.2 Model Predictive Control

Although the time constant of the HVAC system is typically large in most studies, we observe that in our HVAC system, there are both slow modes (time constant ≈ 1200 s) and fast modes (time constant ≈ 10 s) because of the consideration of the enthalpy of evaporation. Therefore, to accurately simulate the responses, we specify the sampling time of the MPC layer ($t_{\mathrm{s,MPC}}$) to be 5 seconds. Simulation time is equal to 9 hours. The number of MPC samples (N) is equal to 6,481 including the initial point. We specify optimization weight matrices

$$Q = \mathbf{I}^{\mathbf{N_P}} \otimes \mathrm{diag}(1, 100),$$

$$R = \mathbf{I}^{\mathbf{N_C}} \otimes \mathrm{diag}(100, 10, 10),$$

where $\mathbf{I^{N_P}}$ and $\mathbf{I^{N_C}}$ are $N_P \times N_P$ and $N_C \times N_C$ identity matrices and $\otimes$ is the Kronecker product operator. We specify input and input increment constraints as follows.

$$\Delta u_{\mathrm{l}} = \begin{bmatrix} -0.005 \\ -31.67 \\ -1.77 \times 10^{-5} \end{bmatrix}, \Delta u_{\mathrm{u}} = \begin{bmatrix} 0.005 \\ 31.67 \\ 1.77 \times 10^{-5} \end{bmatrix},$$

$$u_{\mathrm{l}} = \begin{bmatrix} f_l \\ 0 \\ 0 \end{bmatrix}, u_{\mathrm{u}} = \begin{bmatrix} f_u \\ 2500 \\ -1 \times 10^{-3} \end{bmatrix},$$

By means of (3.14), we obtain

$$u_{\mathrm{l}} - \bar{u} = \begin{bmatrix} f_l - 0.15 \\ -950 \\ -5 \times 10^{-4} \end{bmatrix}, u_{\mathrm{u}} - \bar{u} = \begin{bmatrix} f_u - 0.15 \\ 1550 \\ 5 \times 10^{-4} \end{bmatrix}.$$

We experiment several prediction horizon and control horizon, then yield the superior results with $N_P = 60$ equal to 5 minutes and $N_C = 12$ equal to 1 minute.

4.3.3 Operating Range of Volumetric Flow Rate

Due to Thailand's weather condition, we specify $T_{\mathrm{o,l}} = 25$ °C, $T_{\mathrm{o,h}} = 30$ °C, $\mathrm{RH}_{\mathrm{o,l}} = 40$ %, $\mathrm{RH}_{\mathrm{o,h}} = 90$ %, respectively. Due to the specification of the HVAC system, the operating range of volumetric flow rate is described as follows.

Low to High: the HVAC system maintains volumetric flow rate in a range of 0.12 m^3/s (Low) to 0.18 m^3/s (High).

Medium to High: the HVAC system maintains volumetric flow rate in a range of 0.15 m^3/s (Medium) to 0.18 m^3/s (High).

High: the HVAC system maintains volumetric flow rate at 0.18 m^3/s (High) constantly.

Therefore, Table 3.2 can be rewritten as shown in Table 4.2.

According to examples in Chapter 3, we explain illustrative scenarios as follows.

Table 4.2: Operating range of volumetric flow rate regarding to weather conditions.

	Average humidity		
Average temp.	$\overline{\text{RH}}_\text{o} > 90$ %	40 % $< \overline{\text{RH}}_\text{o} < 90$ %	$\overline{\text{RH}}_\text{o} < 40$ %
$\overline{T}_\text{o} > 30$ °C	0.15 - 0.18	0.18	0.18
25 °C $< \overline{T}_\text{o} < 30$ °C	0.15 - 0.18	0.15 - 0.18	0.15 - 0.18
$\overline{T}_\text{o} < 25$ °C	0.12 - 0.18	0.15 - 0.18	0.15 - 0.18

In summer season, outside temperature is higher than $T_{\text{o,h}}$ whearas outside humidity is in a range of 40% - 90%. Using Table 4.2, we specify 0.18 m^3/s for the operating range of volumetric flow rate.

In rainy season, outside temperature is higher than $T_{\text{o,h}}$ whearas outside humidity is higher than 90%. Thus, the operating range of volumetric flow rate is set in a range of 0.15 to 0.18 m^3/s.

In winter season, outside temperature is lower than $T_{\text{o,l}}$ whereas outside humidity is in a range of 40% - 90%. Therefore, 0.15 to 0.18 m^3/s is recommended for the operating range of volumetric flow rate.

4.3.4 Performance Assessment

To evaluate the performance of the supervisory MPC, we separate performance indices into two parts referring to thermal comfort and peak-load shaving. For the thermal comfort, we define $\Delta T_{\text{Z,rms}}$ as a root-mean-square (RMS) deviation of the zone temperature with respect to T_0, where

$$\Delta T_{\text{Z,rms}} = \sqrt{\frac{\sum_{k=1}^{N}(T_\text{Z}[k] - T_0)^2}{N}}. \tag{4.1}$$

A magnitude of $\Delta T_{\text{Z,rms}}$ implies thermal interference when the zone temperature is lower or greater than the ideal comfort temperature. In parts of peak-load shaving performance, we modify (3.3) by substituting N for N_S and replacing t_s with $t_{\text{s,MPC}}$. In the following sections, we will use these indices to evaluate the results.

4.4 Illustrative Examples

In this section, we demonstrate an application of the proposed supervisory MPC to three cases of weather conditions in Thailand, namely, summer season, winter season, and rainy season.

4.4.1 Summer Season

To simulate heat and humidity load profile, we consider a typical day in summer season with working hours from 8:00–17:00. In this example, a human metabolism generates heat of $1,500$ Kcal/day or 72.57 W [28] and a human respiration generates water vapor of 0.08 kg/h or 2.22×10^{-5} kg/s [21]. Let N_{oc} be the number of occupants. We calculate hourly heat (W) and humidity load (kg/h) by

$$Q_{\text{L}} = 72.57 \cdot N_{\text{oc}},$$

$$\omega_{\text{L}} = 2.22 \times 10^{-5} \cdot N_{\text{oc}}.$$

The numbers of occupants per hour are given in Table 4.3.

Table 4.3: The hourly number of occupants.

Time (hour)	8	9	10	11	12	13	14	15	16	17
N_{oc}	4	5	6	6	7	7	6	6	5	4

After computing Q_{L} and ω_{L}, we perform a polynomial interpolation on the data using `spline` in `MATLAB` [29]. The interpolated disturbance profile is illustrated in Figure 4.5.

Using the above settings, we can compute **OptRef**. In Figure 4.6, We compare **OptRef**, generated by the SC layer, using different volumetric flow rate. Using higher volumetric flow rate allows us to use higher set-point temperature resulted increase of electrical power reduction and TOC reduction.

We explore a trade-off performance between J_{TOC} and J_{TCC} in the SC layer. To

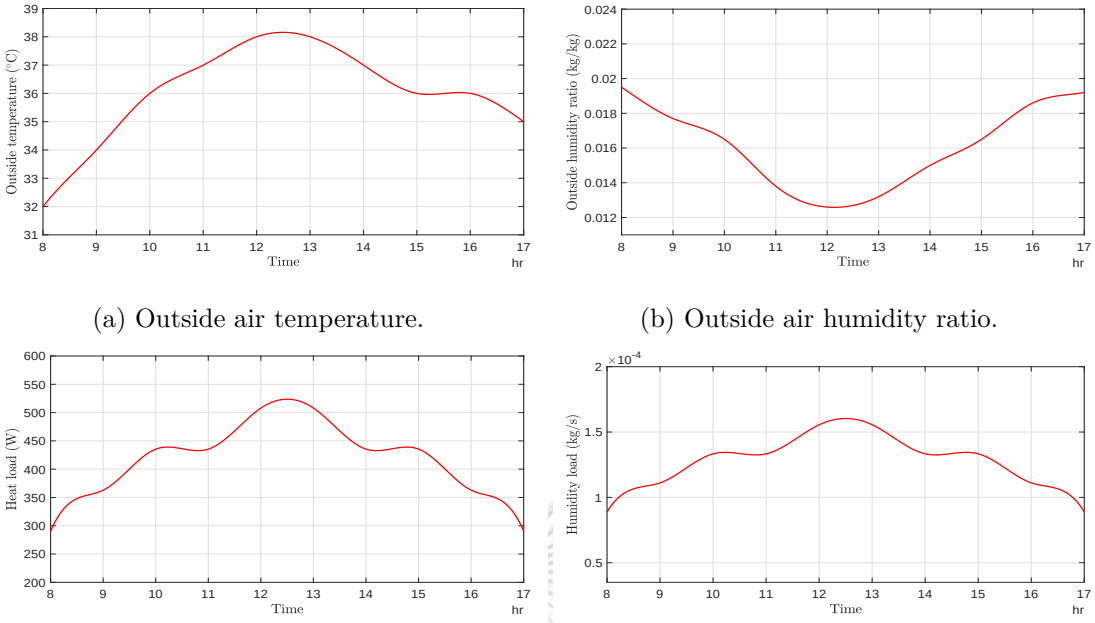

(a) Outside air temperature.

(b) Outside air humidity ratio.

(c) Heat load.

(d) Humidity load.

Figure 4.5: Interpolated disturbances profile used in the simulations.

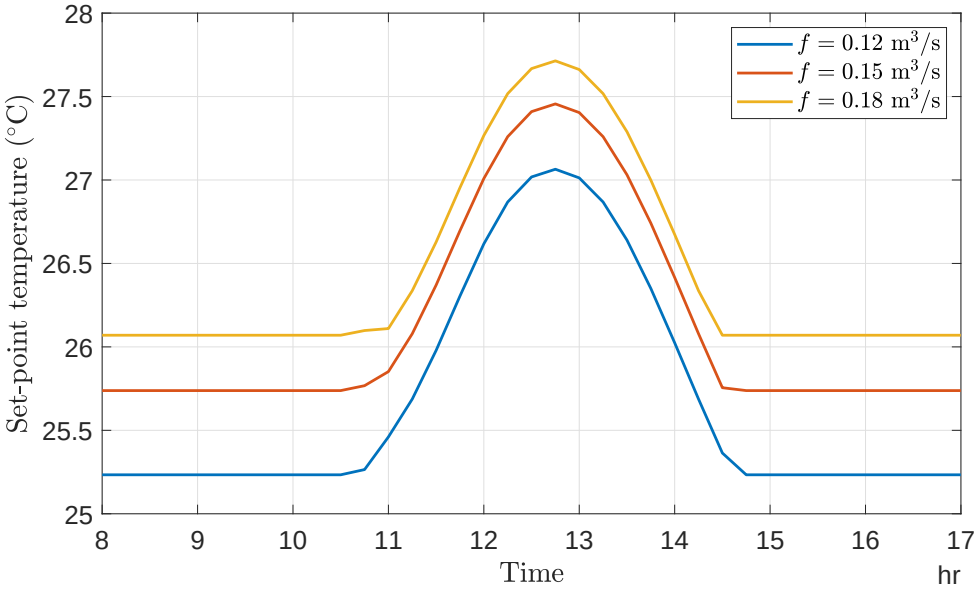

Figure 4.6: Optimal reference temperature (**OptRef**) in summer season.

Figure 4.7: Trade-off between TOC and TCC in summer season.

demonstrate the trade-off performance, we compute the optimal solution by varying the value of α in (3.10) from 0 to 1. We then obtain the Pareto optimal curve as shown in

Fig. 4.7. The results show the trade-off performance between J_{TOC} and J_{TCC} where the maximum of the J_{TOC} and the maximum of the J_{TOC} are equal to 1. We observe that the Pareto optimal front occurs when α is equal to 0.5. This implies the value of J_{TCC} cannot be made smaller without allowing the value of J_{TOC} to increase.

In comparison to other references, we choose three conventional reference patterns, namely, **Nom**, **Step**, and **Trapz**. A comparison of these references are shown in Figure 4.8. We describe patterns of **Nom**, **Step**, and **Trapz** as follows.

Nom: This set-point profile is a nominal operation used to compare control performance of each case. T_{ref} is constant at 26.03 °C for all times.

Step: This set-point profile is adapted from [24]. We increase the set-point temperature from 26.03 °C to 27.71 °C when the peak-load of the nominal operation occurs. We observe the power profile of the nominal operation and choose to step up the set-point temperature at 10:45 and step down at 14:30.

Trapz: In the same way as **Step**, we increase T_{ref} from 26.03 °C to 27.71 °C to shave the peak-load. The set-point temperature changing function is a trapezoidal function with ramp time = 30 minute which starts the ramp-up at 10:45 and starts the ramp-down at 14:00.

For all comparisons, ω_{ref} is 0.012 kg/kg which is equivalent to the zone relative humidity at 54.5%. Additionally, we relax the volumetric flow rate in MPC design (3.13) with **Nom**, **Step**, and **Trapz** by selecting $f_{\text{l}} = 0.12$ m^3/s while keeping $f_{\text{u}} = 0.18$ m^3/s. The purpose of constraint relaxation is to enlarge the feasible region of the MPC design problem to achieve the better cost of the MPC and to show an importance on selection of the volumetric flow rate.

Computing from disturbances profile, we obtain $\overline{T}_{\text{o}} = 36.60$ °C and $\overline{\text{RH}}_{\text{o}} = 54.2$ %. Regarding to Table 4.2, it suggests us to choose a range of operating flow rate to be **High** where $f_{\text{l}} = 0.18$ kg/kg and $f_{\text{u}} = 0.18$ kg/kg. Therefore, (3.14) can be expressed

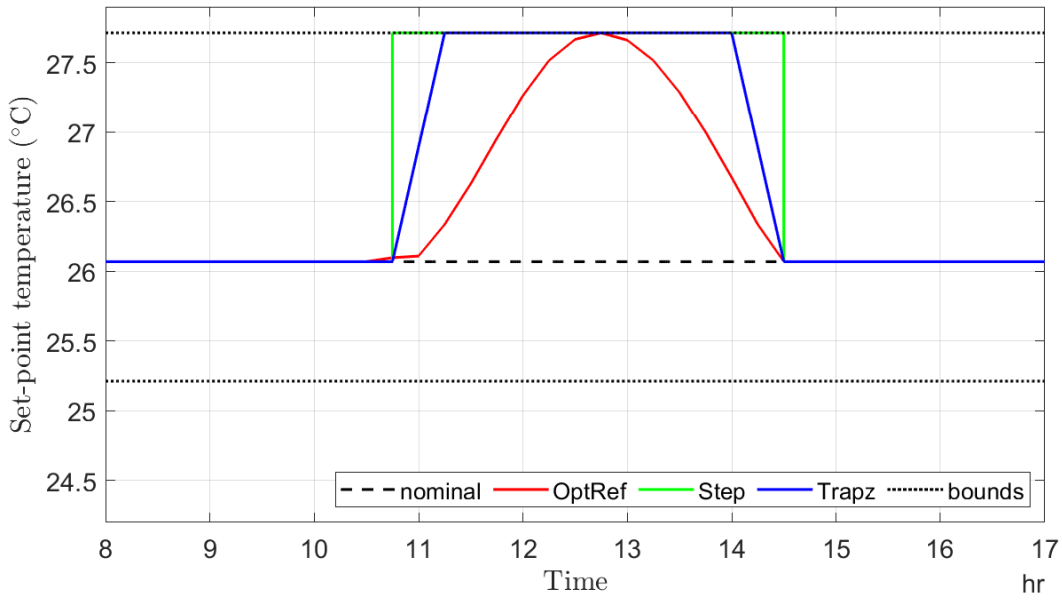

Figure 4.8: Different references in summer season.

as

$$u_{\mathrm{l}} - \bar{u} = \begin{bmatrix} 0.03 \\ -950 \\ -5 \times 10^{-4} \end{bmatrix}, u_{\mathrm{u}} - \bar{u} = \begin{bmatrix} 0.03 \\ 1550 \\ 5 \times 10^{-4} \end{bmatrix}.$$

Consequently, output responses and input responses from the MPC layer are shown in the following figures.

Firstly, we observe in Figure 4.9 that zone temperature from the MPC can track its set-point efficiently. In Figure 4.10, there is a swing of zone RH during set-point temperature changing phase in cases of **Step** and **Trapz** whereas **OptRef** generates only small deviation of zone RH from set-point humidity ratio. This is because **OptRef** has a slow-changing characteristic. In parts of control inputs, we observe that the peak of heat exchanger electrical power is smoothly shaved by **OptRef**. Peak electrical power is reduced by 13.43 % compared to the nominal case.

As results of the control design, **OptRef** gives the best result on TOC reduction. Temperature deviation from T_{o} from **OptRef** is the smallest compared to the others. This implies less thermal comfort violation generated from **OptRef**. Lastly, PMV, shown in Figure 4.16, is well-regulated with the help of specification of the volumetric

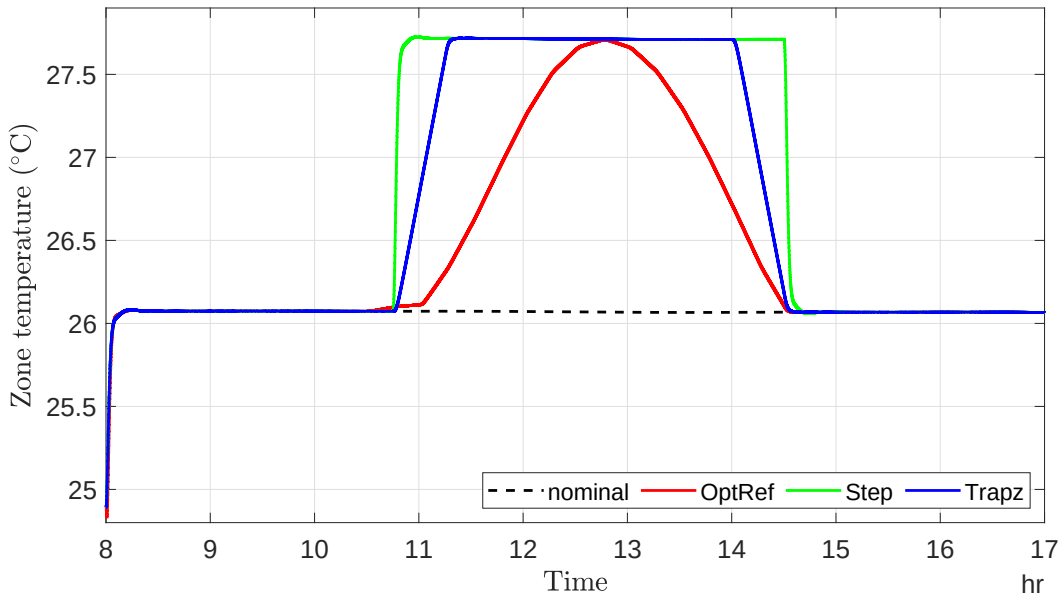

Figure 4.9: Zone temperature in summer season.

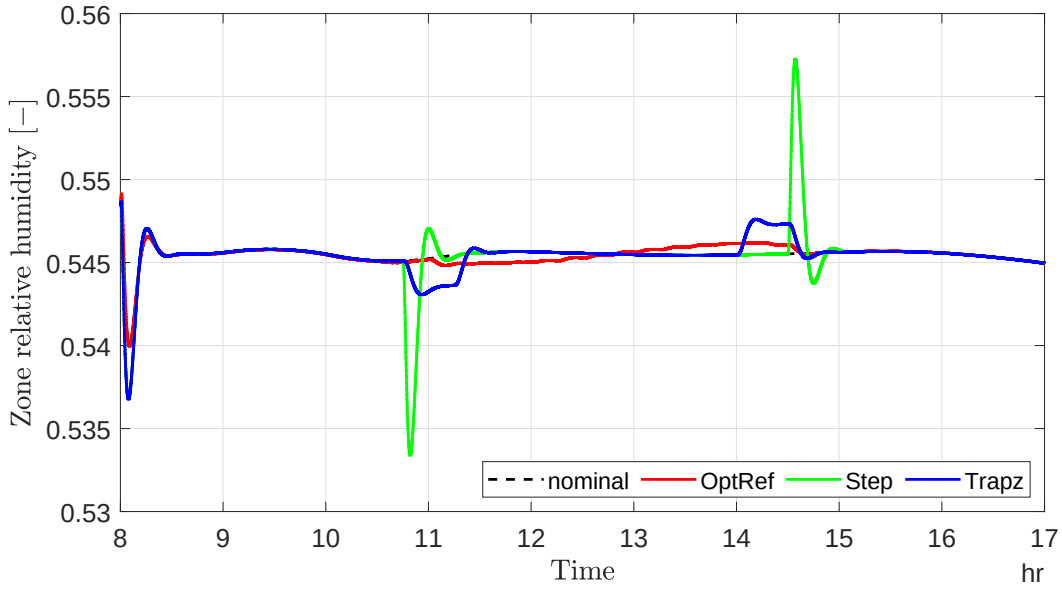

Figure 4.10: Zone relative humidity in summer season.

flow rate constraint.

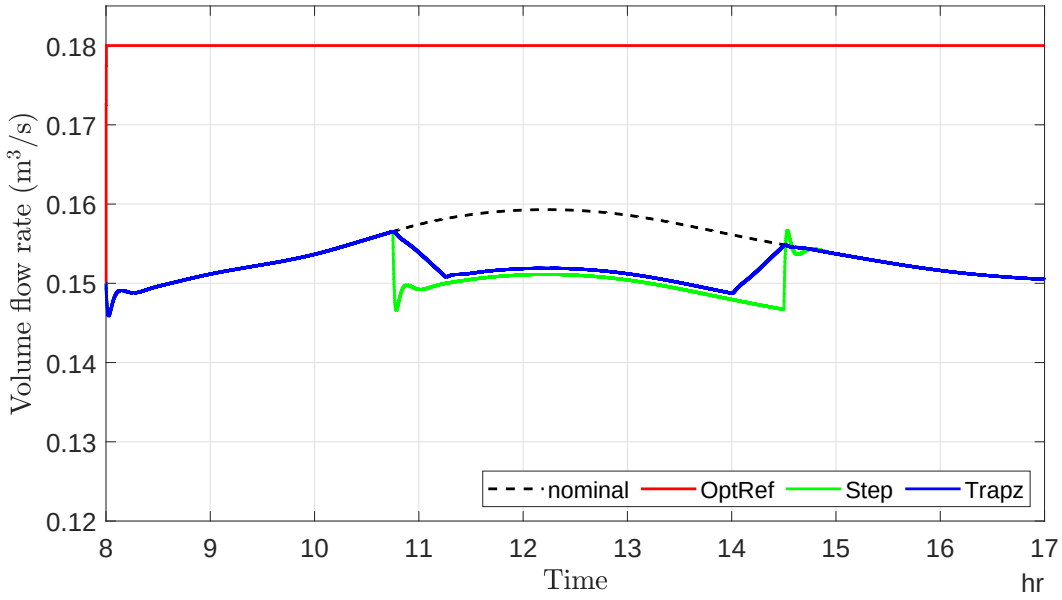

Figure 4.11: Volumetric flow rate in summer season.

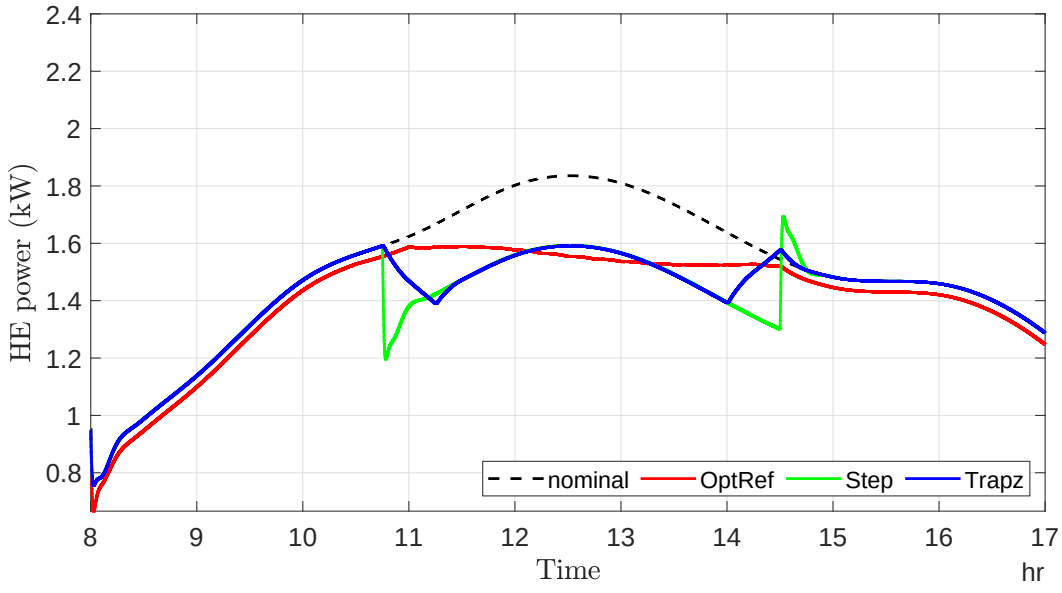

Figure 4.12: Heat exchanger electrical power in summer season.

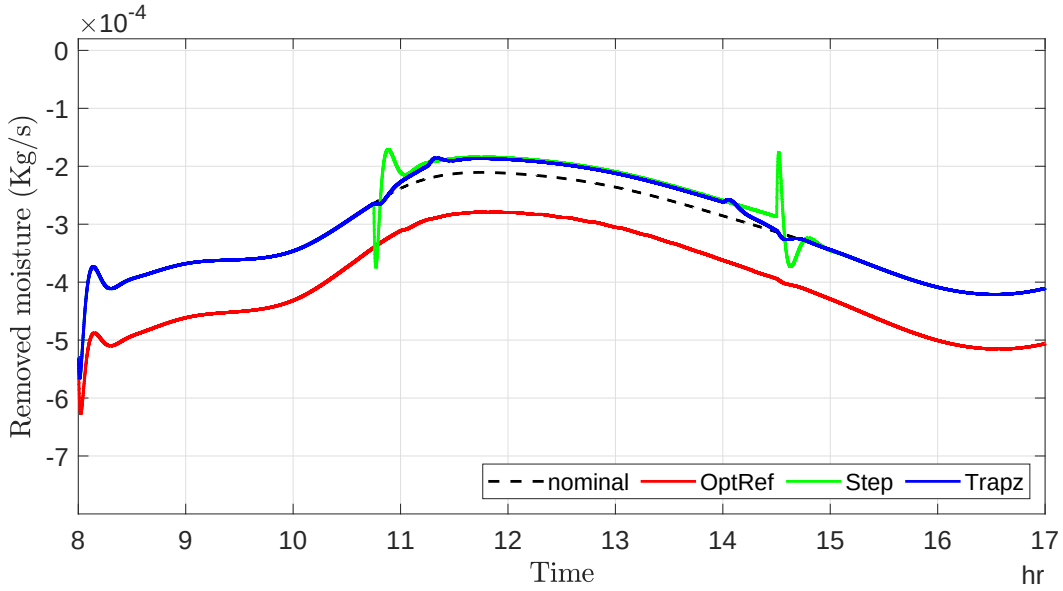

Figure 4.13: Removed moisture in summer season.

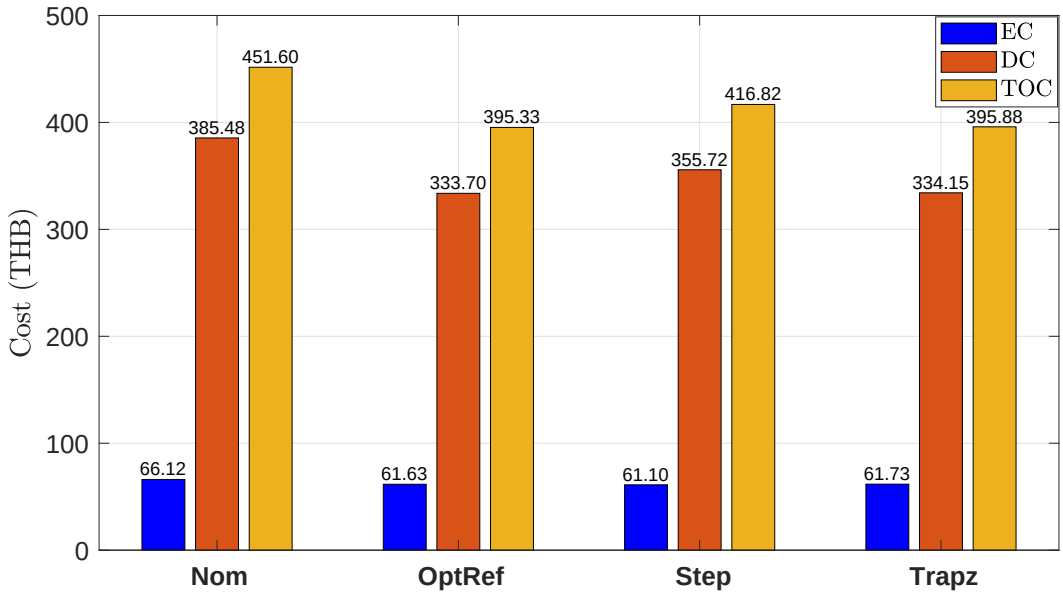

Figure 4.14: TOC in summer season.

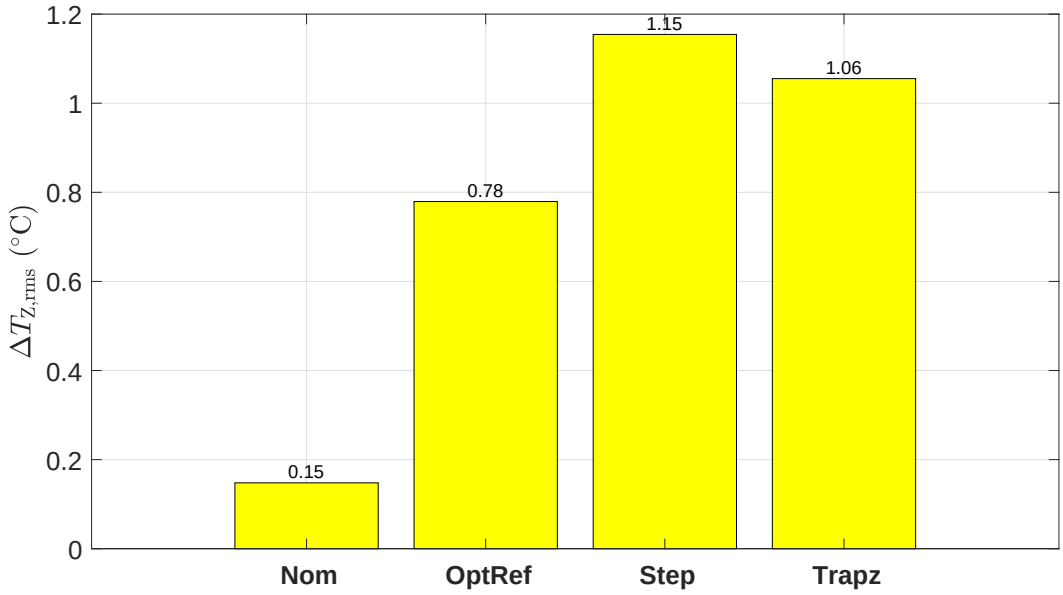

Figure 4.15: TCC in summer season.

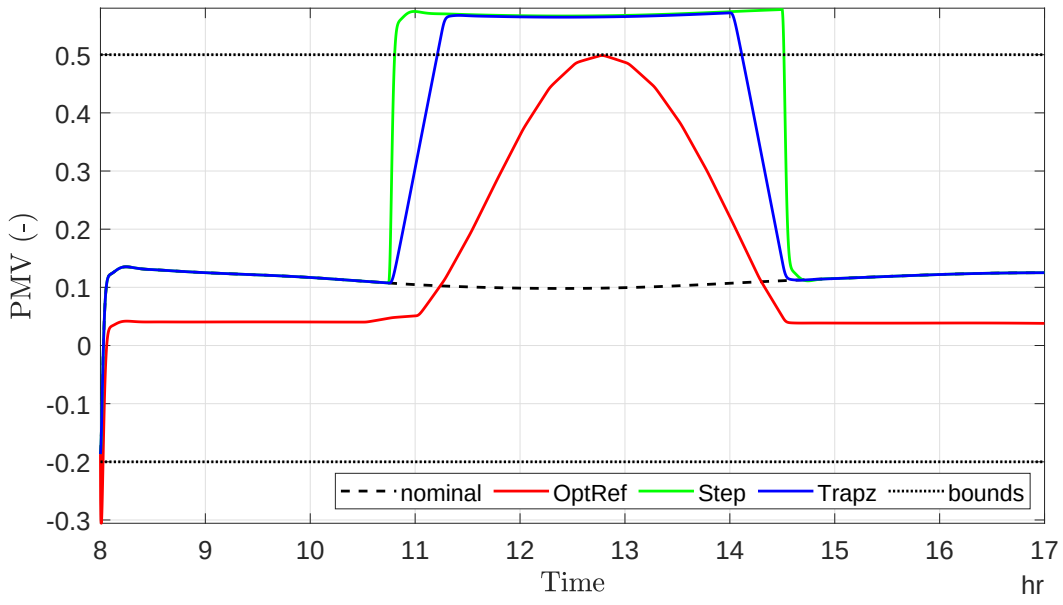

Figure 4.16: Zone PMV in summer season.

4.4.2 Rainy Season

In the experiments, we select September 23, 2019 for an example. A weather profile is shown in Figure 4.17.

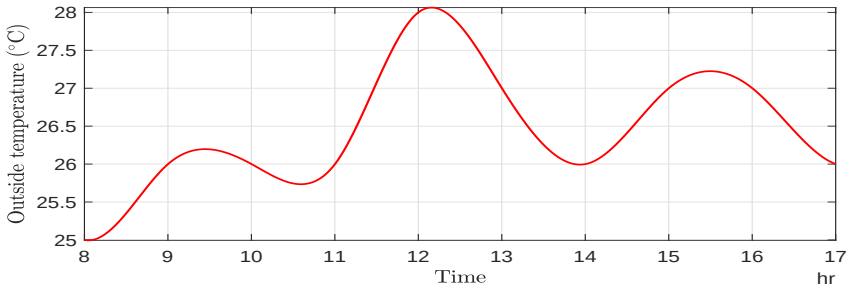

(a) Outside air temperature.

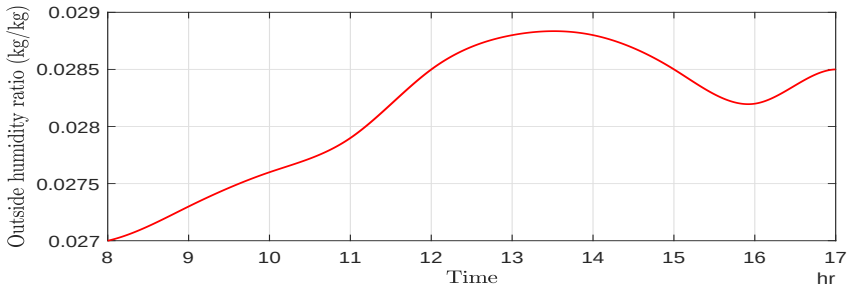

(b) Outside air humidity ratio.

Figure 4.17: Interpolated disturbances profile used in the simulations in rainy season.

A rainfall during 12:30-14:00 caused the outside air temperature drops from 28 °C to 26 °C. When the rainfall is end, we observe that the outside air temperature rises up. Thus, we foresee that there will occur another peak-load around 15:30. In parts of the outside humidity, we observe that the outside air humidity ratio is in a range of 0.027 kg/kg to 0.029 kg/kg which is dramatically greater than the operating humidity ratio (0.012 kg/kg).

Using the above settings, we can compute **OptRef**. In Figure 4.18, We compare **OptRef**, generated by the SC layer, using different volumetric flow rate. Using higher volumetric flow rate allows us to use higher set-point temperature resulted increase of electrical power reduction and TOC reduction. However, we suggest to set the volumetric flow rate at medium to high level in rainy season since using high flow rate may

cause loss in humidity control.

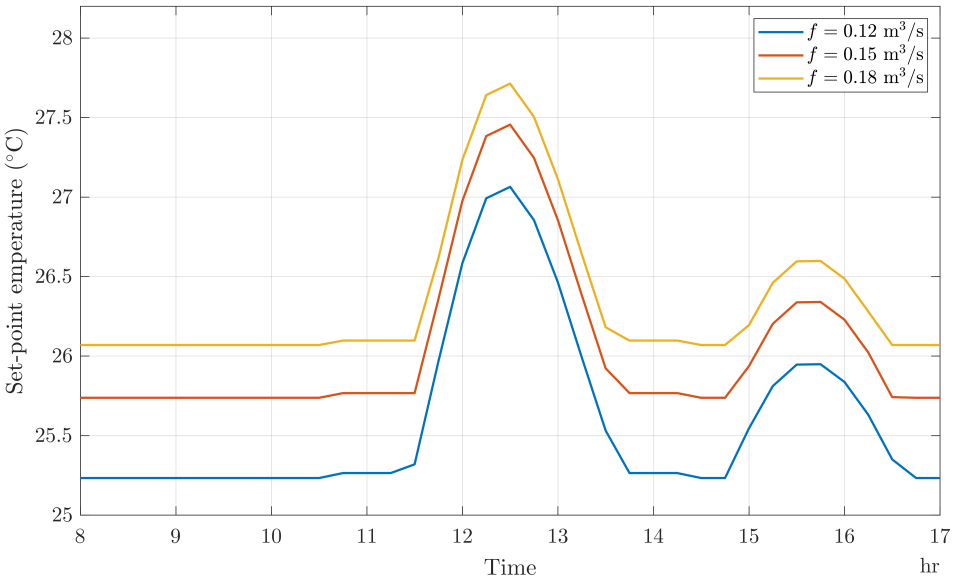

Figure 4.18: Optimal reference temperature (**OptRef**) in rainy season.

Figure 4.19: Trade-off between TOC and TCC in rainy season.

We explore a trade-off performance between J_{TOC} and J_{TCC} in the SC layer. To demonstrate the trade-off performance, we compute the optimal solution by varying the value of α in (3.10) from 0 to 1. We then obtain the Pareto optimal curve as shown in Fig. 4.19. The results show the trade-off performance between J_{TOC} and J_{TCC} where the maximum of the J_{TOC} and the maximum of the J_{TOC} are equal to 1. In the same way as in summer season, we observe that the Pareto optimal front occurs when α is equal to 0.5. This implies the value of J_{TCC} cannot be made smaller without allowing the value of J_{TOC} to increase.

In comparison to other references, we choose three conventional reference patterns, namely, **Nom**, **Step**, and **Trapz**. A comparison of these references are shown in Figure 4.20. We describe patterns of **Nom**, **Step**, and **Trapz** as follows.

Nom: This set-point profile is a nominal operation used to compare control performance of each case. T_{ref} is constant at 25.74 °C for all times.

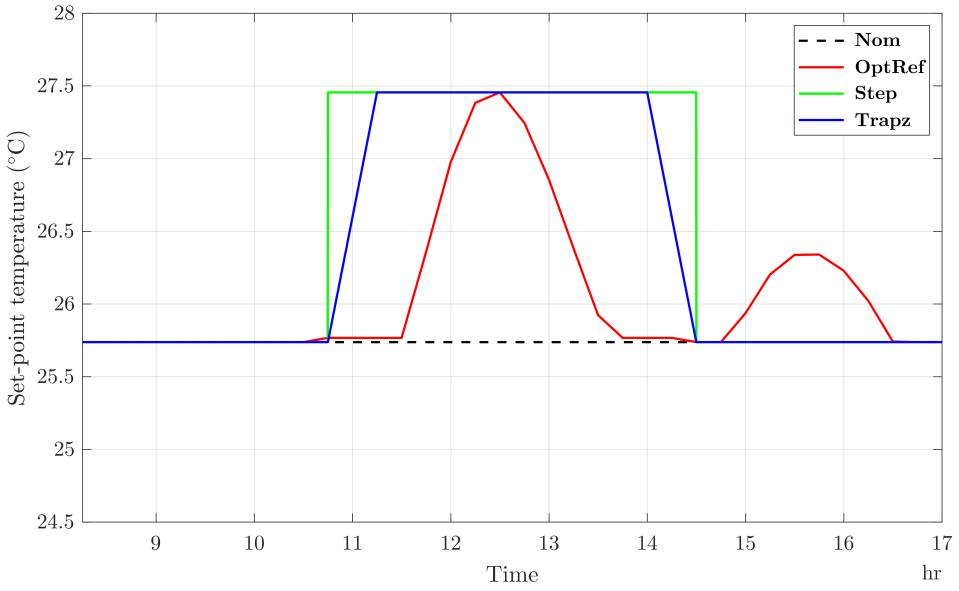

Figure 4.20: Different references in rainy season.

Step: This set-point profile is adapted from [24]. We increase the set-point temperature from 25.74 °C to 27.46 °C when the peak-load of the nominal operation occurs. We observe the power profile of the nominal operation and choose to step up the set-point temperature at 10:45 and step down at 14:30.

Trapz: In the same way as **Step**, we increase T_{ref} from 25.74 °C to 27.47 °C to shave the peak-load. The set-point temperature changing function is a trapezoidal function with ramp time = 30 minute which starts the ramp-up at 10:45 and starts the ramp-down at 14:00.

For all comparisons, ω_{ref} is 0.012 kg/kg which is equivalent to the zone relative humidity at 54.5%. Additionally, we relax the volumetric flow rate in MPC design (3.13) with **Nom**, **Step**, and **Trapz** by selecting $f_{\text{l}} = 0.12$ m^3/s while keeping $f_{\text{u}} = 0.18$ m^3/s. The purpose of constraint relaxation is to enlarge the feasible region of the MPC design problem to achieve the better cost of the MPC and to show an importance on selection of the volumetric flow rate.

Computing from disturbances profile, we obtain $\overline{T}_{\text{o}} = 26.40$ °C and $\overline{\text{RH}}_{\text{o}} = 93.70$ %. Regarding to Table 4.2, it suggests us to choose a range of operating flow

rate to be **High** where $f_{\mathrm{l}} = 0.15$ kg/kg and $f_{\mathrm{u}} = 0.18$ kg/kg. Therefore, (3.14) can be expressed as

$$u_{\mathrm{l}} - \bar{u} = \begin{bmatrix} 0 \\ -950 \\ -5 \times 10^{-4} \end{bmatrix}, u_{\mathrm{u}} - \bar{u} = \begin{bmatrix} 0.03 \\ 1550 \\ 5 \times 10^{-4} \end{bmatrix}.$$

Consequently, output responses and input responses from the MPC layer are shown in the following figures.

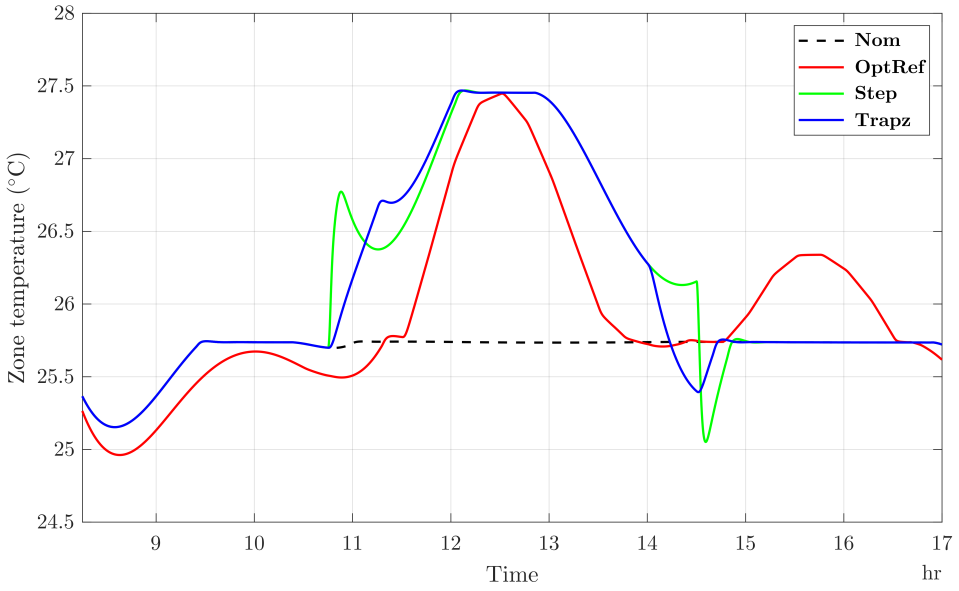

Figure 4.21: Zone temperature in rainy season.

From the results, we observe that **OptRef** tends to follow a pattern of the outside air temperature. With the fast-changing set-point temperatures such as **Step** and **Trapz**, MPC fails to regulate the zone RH around 54.5 %. In addition, there occurs some oscillations of the zone temperatures during the ramp period. Unlike the slow-changing rate set-point, **OptRef** helps the MPC to accurately maintain both the zone temperature and zone humidity ratio around the given set-point.

In parts of control inputs, with the knowledge on disturbances profile, **OptRef** efficiently entirely shaves the heat exchanger electrical power. Although **OptRef** only reduces the first peak-load by 57.95 % worse than 67.59 % from **Step** and 67.83 % from **Trapz**, the second peak-load, occured when the rainfall ends, from **OptRef** is reduced

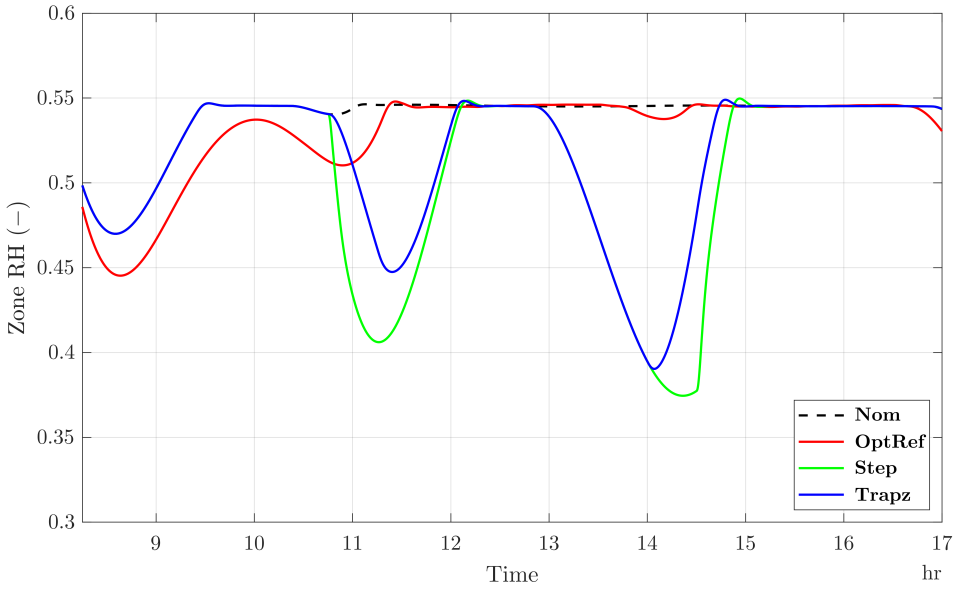

Figure 4.22: Zone RH in rainy season.

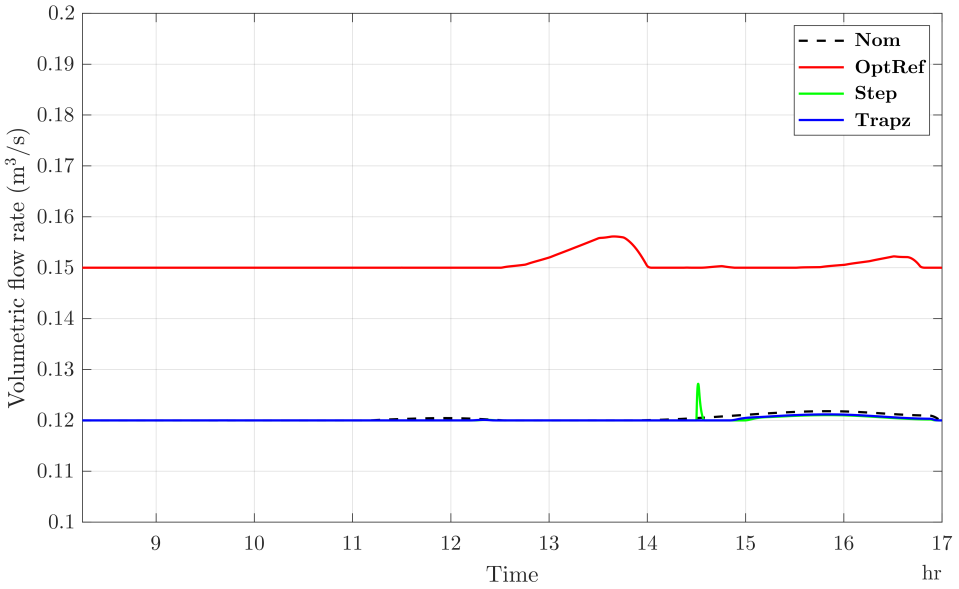

Figure 4.23: Volumetric flow rate in rainy season.

by 51.88 % compared to the other cases. This makes the peak-load during the daytime of **OptRef** be in the best position (158 W) compared to **Step** (205.4 W) and **Trapz** (205.4 W).

As a result, we compare EC, DC, and TOC of **OptRef** shown in Figure 4.26

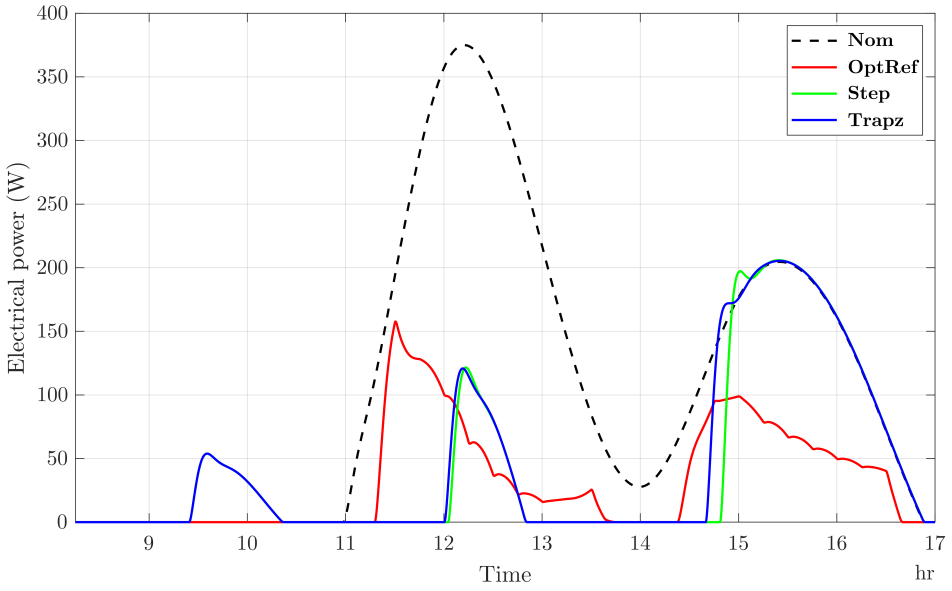

Figure 4.24: Heat exchanger electrical power in rainy season.

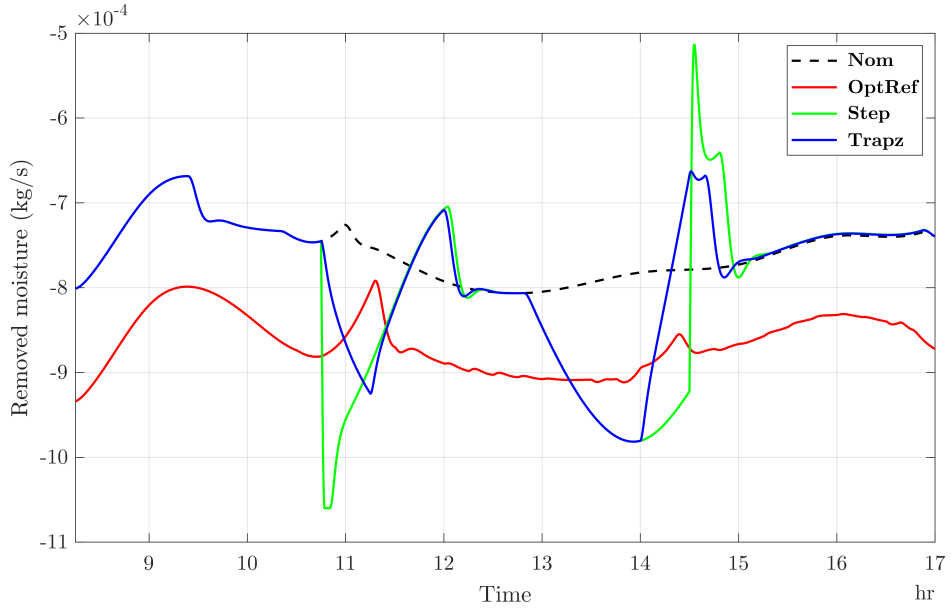

Figure 4.25: Removed moisture in rainy season.

is reduced by 58.88 % compare to 46.44 % of **Step** and 46.43 % **Trapz**. However, we observe the better performance of **Trapz** when we consider on thermal comfort regulation. Figure 4.27 shows that **OptRef** generates 0.80 °C of the deviation whearas both **Step** and **Trapz** lead to 0.89 °C and 0.71 °C, respectively.

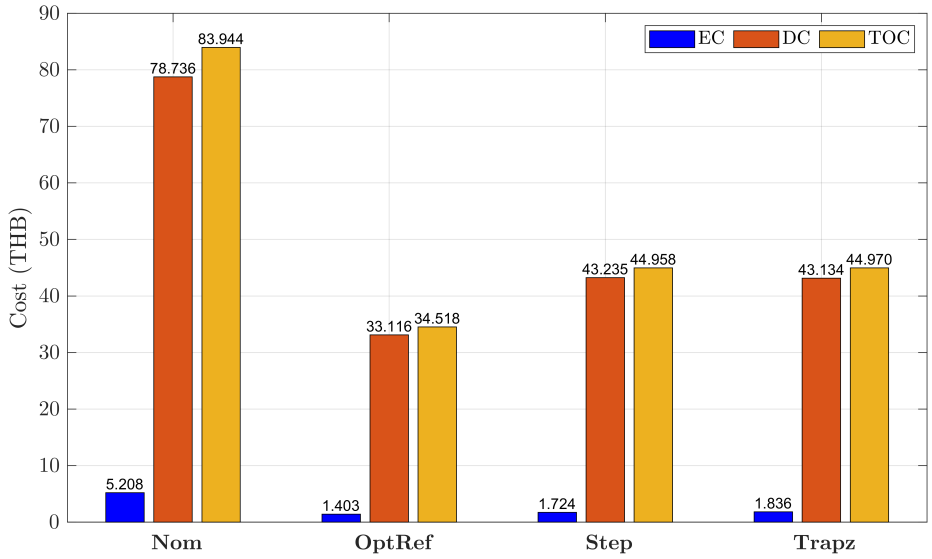

Figure 4.26: TOC in rainy season.

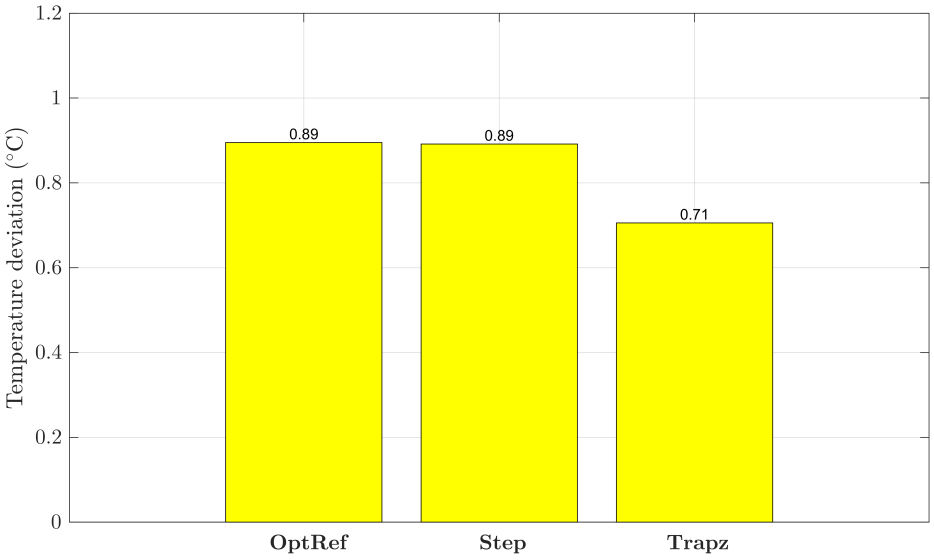

Figure 4.27: Temperature deviation in rainy season.

Lastly, using **OptRef** with the MPC gives the PMV, shown in Figure 4.28, within the defined region whearas the others fail to regulated the PMV.

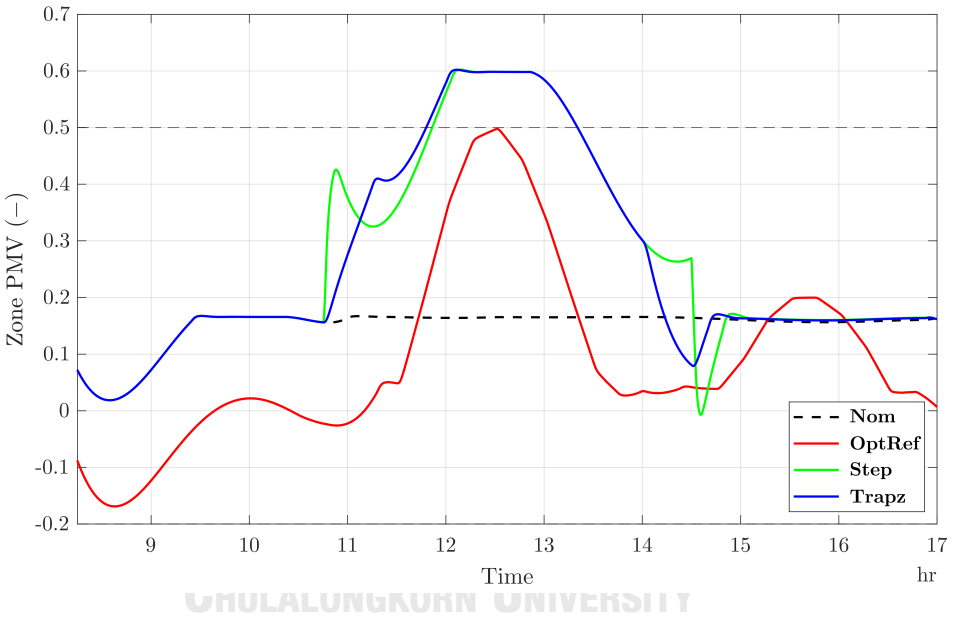

Figure 4.28: Zone PMV in rainy season.

4.4.3 Winter Season

We choose the date Jan 3, 2019 as our example of the date in winter season. The outside air temperature and the outside air humidity ratio are shown in Figure 4.29.

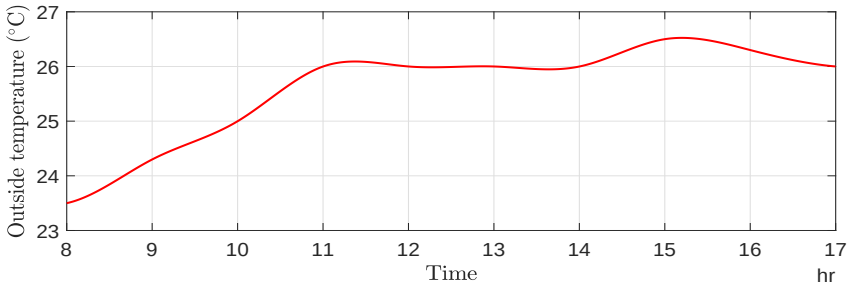

(a) Outside air temperature.

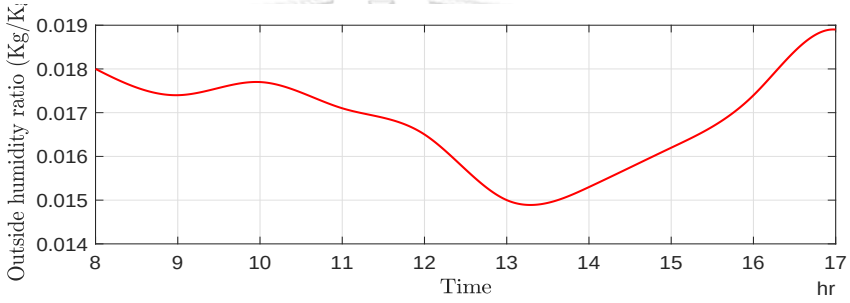

(b) Outside air humidity ratio.

Figure 4.29: Interpolated disturbances profile for winter used in the simulations.

We observe that the outside air temperature during the morning of the day is lower than 25 °C which is the operating temperature. Since our HVAC system is specified to operate in the cooling mode, we then suggest that the HVAC system should be turned-off during 8:00 to 10:00. After 10:00, we initialize the HVAC system and the supervisory MPC to design **OptRef**. For an internal load, we asssume that the occupied period of the zone remains the same as Table 4.3. Therefore, heat load and humidity load generated by occupants are the same as shown in Figures 4.5c and 4.5d.

Using the above settings, we can compute **OptRef**. In Figure 4.30, We compare **OptRef**, generated by the SC layer, using different volumetric flow rate. Using higher volumetric flow rate allows us to use higher set-point temperature resulted increase of

electrical power reduction and TOC reduction.

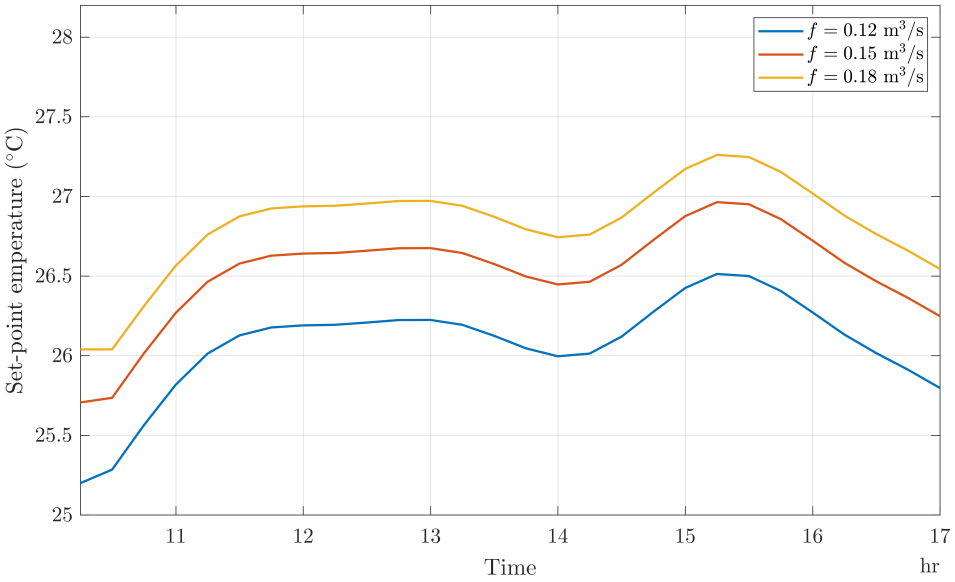

Figure 4.30: Optimal reference temperature (**OptRef**) in winter season.

Figure 4.31: Trade-off between TOC and TCC in winter season.

We explore a trade-off performance between J_{TOC} and J_{TCC} in the SC layer. To demonstrate the trade-off performance, we compute the optimal solution by varying the value of α in (3.10) from 0 to 1. We then obtain the Pareto optimal curve as shown in Fig. 4.31. The results show the trade-off performance between J_{TOC} and J_{TCC} where the maximum of the J_{TOC} and the maximum of the J_{TOC} are equal to 1. In the same way as in summer season, we observe that the Pareto optimal front occurs when α is equal to 0.5. This implies the value of J_{TCC} cannot be made smaller without allowing the value of J_{TOC} to increase.

In comparison to other references, we choose three conventional reference patterns, namely, **Nom**, **Step**, and **Trapz**. A comparison of these references are shown in Figure 4.8. We describe patterns of **Nom**, **Step**, and **Trapz** as follows.

Nom: This set-point profile is a nominal operation used to compare control performance of each case. T_{ref} is constant at 25.71 °C for all times.

Step: This set-point profile is adapted from [24]. We increase the set-point temperature from 25.71 °C to 27.46 °C when the peak-load of the nominal operation occurs. We observe the power profile of the nominal operation and choose to step up the set-point temperature at 10:45 and step down at 14:30.

Trapz: In the same way as **Step**, we increase T_{ref} from 25.71 °C to 27.46 °C to shave the peak-load. The set-point temperature changing function is a trapezoidal function with ramp time = 30 minute which starts the ramp-up at 10:45 and starts the ramp-down at 14:00.

For all comparisons, ω_{ref} is 0.012 kg/kg which is equivalent to the zone relative humidity at 54.5%. Additionally, we relax the volumetric flow rate in MPC design (3.13) with **Nom**, **Step**, and **Trapz** by selecting $f_{\text{l}} = 0.12$ m^3/s while keeping $f_{\text{u}} = 0.18$ m^3/s. The purpose of constraint relaxation is to enlarge the feasible region of the MPC design problem to achieve the better cost of the MPC and to show an importance on selection of the volumetric flow rate.

Computing from disturbances profile, we obtain $\overline{T}_{\text{o}} = 25.56$ °C and $\overline{\text{RH}}_{\text{o}} = 56.4$ %. Regarding to Table 4.2, it suggests us to choose a range of operating flow rate to be **High** where $f_{\text{l}} = 0.15$ kg/kg and $f_{\text{u}} = 0.18$ kg/kg. Therefore, (3.14) can be expressed as

$$u_{\text{l}} - \bar{u} = \begin{bmatrix} 0 \\ -950 \\ -5 \times 10^{-4} \end{bmatrix}, u_{\text{u}} - \bar{u} = \begin{bmatrix} 0.03 \\ -950 \\ -5 \times 10^{-4} \end{bmatrix}.$$

Consequently, output responses and input responses from the MPC layer are shown in the following figures.

From the results, we observe that **OptRef** follows the trend of the outside air temperature. In parts of control inputs, the heat exchanger electrical power from **OptRef** is nearly zero which also gives the minimum of the TOC. This means operating the HVAC system only in the fan mode is enough to control the thermal comfort of the occupants and also gives the minimum of the TOC.

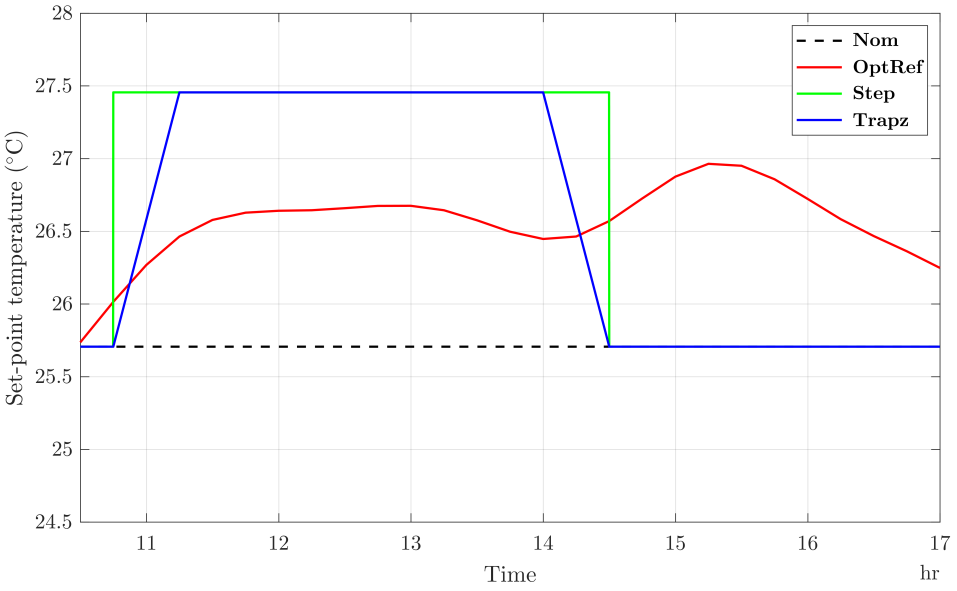

Figure 4.32: Different references in winter season.

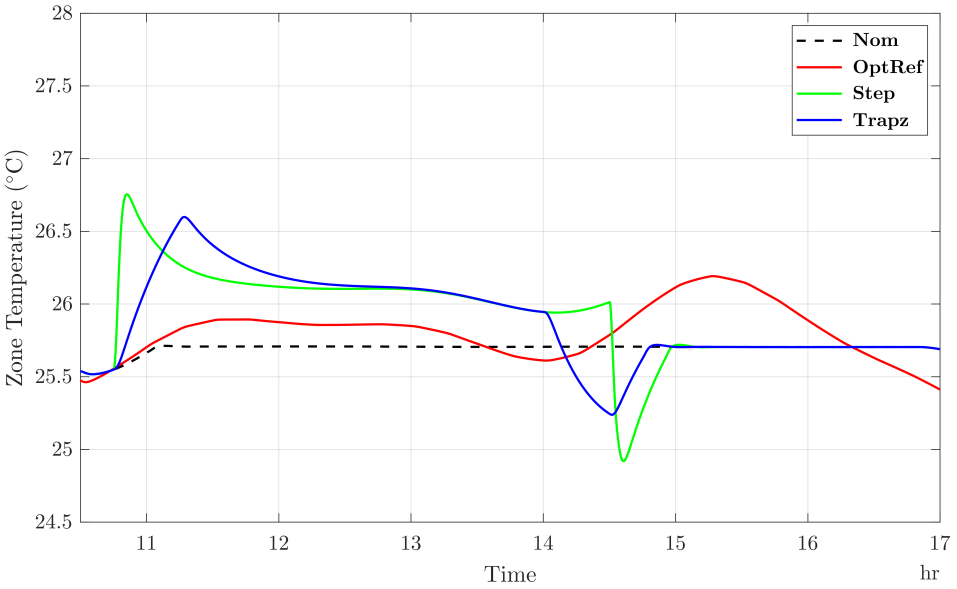

Figure 4.33: Zone temperature in winter season.

In opposite to the experiments in rainy season, **OptRef** in winter season give the best attainable TOC reduction whereas the trade-off on the deviation of zone temperatures is observed. In Figure 4.38, TOC generated by **OptRef** is equal to 0 which is significantly reduced compared to the other cases. On the other hand, we can see in Figure 4.39 that **OptRef** generates 0.44 °C of temperature deviation which is higher

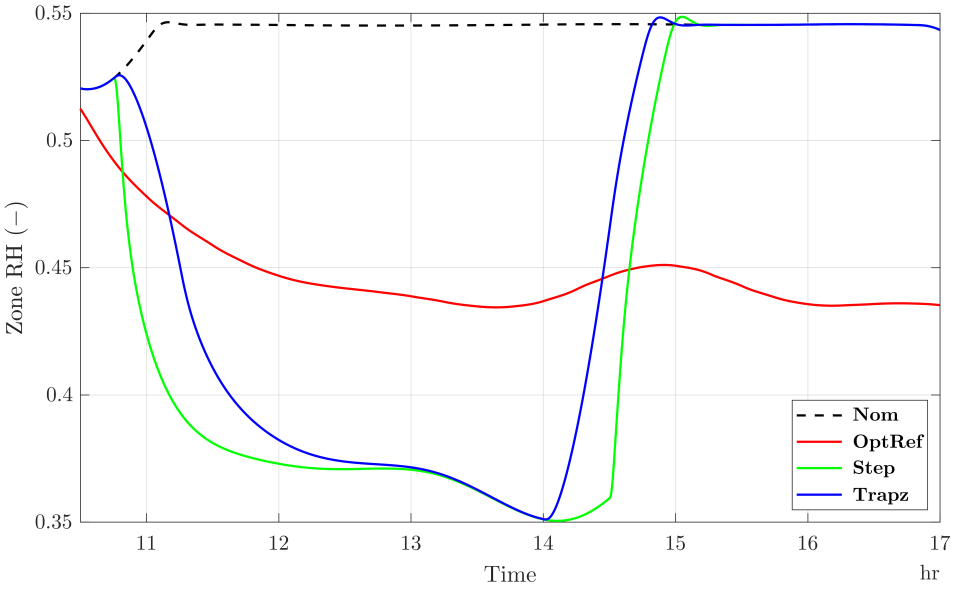

Figure 4.34: Zone RH in winter season.

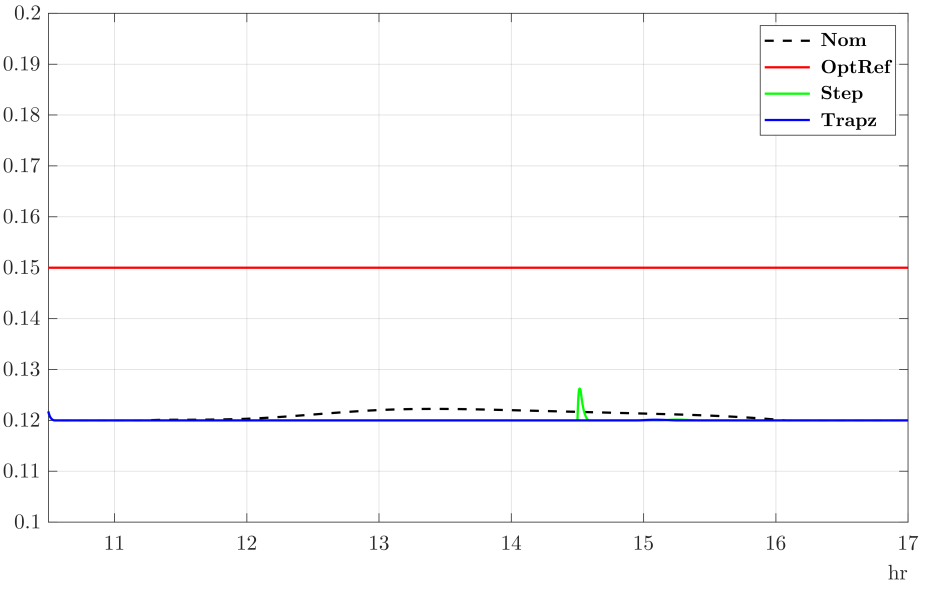

Figure 4.35: Volumetric flow rate in winter season.

than both 0.43 °C from **Step** and 0.29 °C from **Trapz**. By the way, there is PMV violation in all cases as in Figure 4.40.

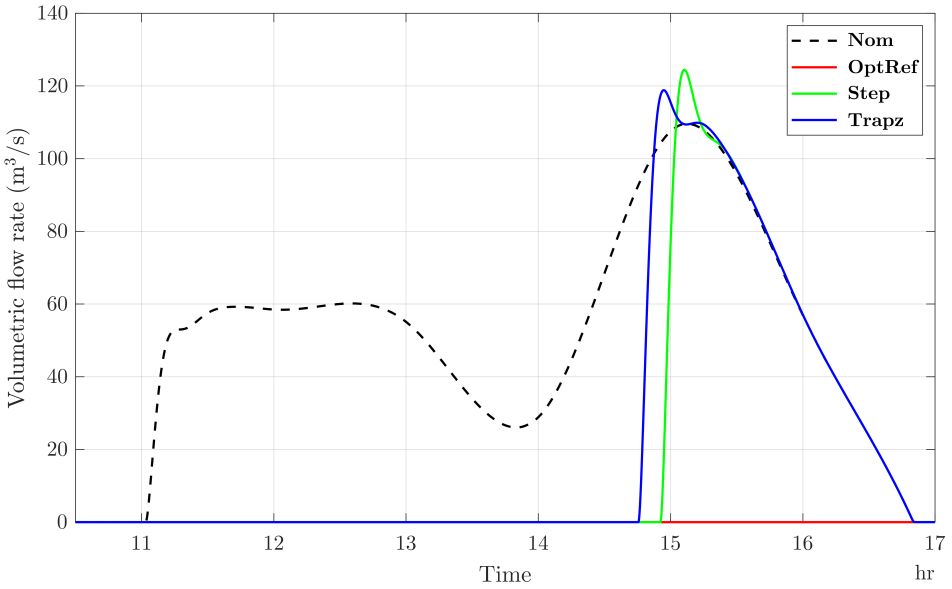

Figure 4.36: Heat exchanger electrical power in winter season.

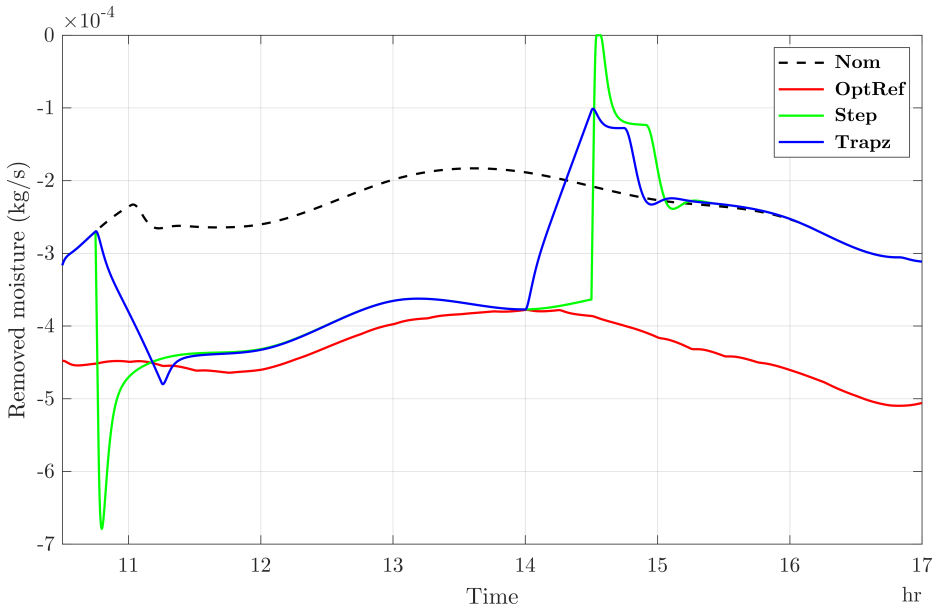

Figure 4.37: Removed moisture in winter season.

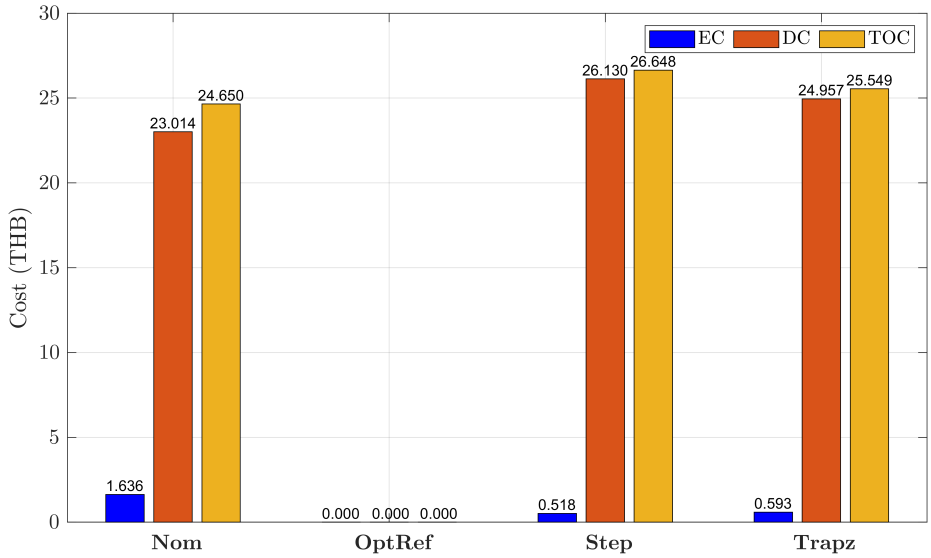

Figure 4.38: TOC in winter season.

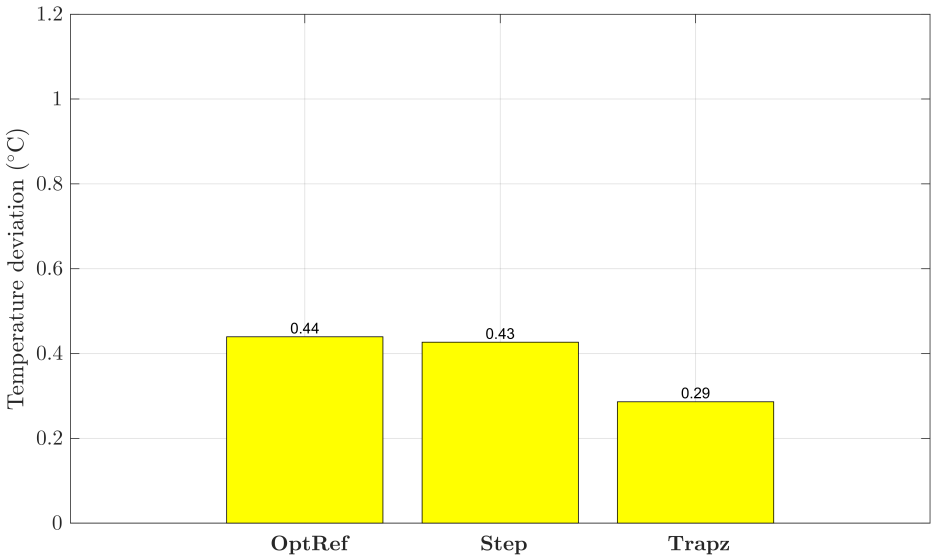

Figure 4.39: Temperature deviation in winter season.

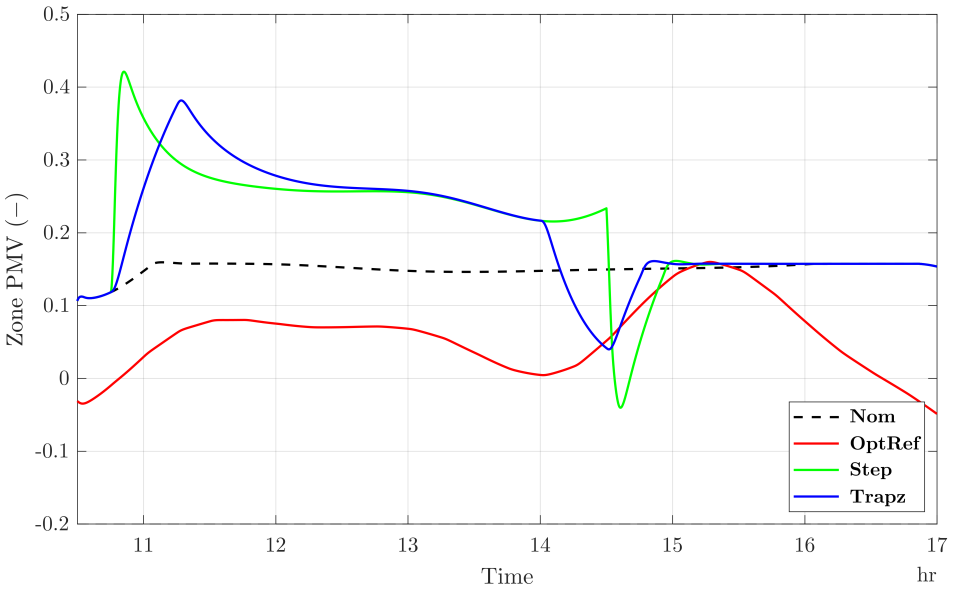

Figure 4.40: Zone PMV in winter season.

4.5 Discussion

According to our numerical results, Table 4.4 summarize performance of the proposed control design under various weather conditions.

Table 4.4: Performance of using **OptRef** under various weather conditions.

Case		Performance indices		
		Peak-load	TOC	Temperature deviation (°C)
Summer	**Nom**	1835.6 W	451.6 THB	0 °C
	OptRef	1589.0 W	395.33 THB	0.78 °C
	change	-13.43%	-12.46%	+0.78 °C
Rainy	**Nom**	374.9 W	83.94 THB	0 °C
	OptRef	157.7 W	34.52 THB	0.89 °C
	change	-57.95%	-58.9%	+0.89 °C
Winter	**Nom**	109.6 W	24.65 THB	0 °C
	OptRef	0	0 THB	0.44 °C
	change	-100%	-100%	+0.44 °C

Generally, **OptRef** succesfully reduces electrical peak-load during the day. Peak-load is reduced by 13.43% in summer season, 57.95% in rainy season. In winter season, heat exchanger can be turned-off while HVAC system is operating in fan-mode.

In terms of cost saving, **OptRef** in the summer season yields the best cost saving in THB, following by that in rainy season, and that in winter season, orderly. When compared to the other seasons, we observe that **OptRef** gives a significant TOC reduction in rainy season because of the detection of second peak-load. In terms of themal comfort interference, temperature deviation is less than 1 °C. This implies thermal comfort is well-regulated. As results, we ensure that the proposed supervisory MPC can be implemented and operated in various operating conditions.

To state the contribution of the proposed supervisory MPC, we point out advantages of our control design as follows. Firstly, we integrate outside air temperature and

heat load into the SC layer, so the set-point temperature of **OptRef** adapts itself to the environmental condition. We observe that the set-point temperature **OptRef** follows the change of specific disturbances, the outside temperature and heat load. This means **OptRef** is more adaptable with disturbance patterns than **Step** and **Trapz**.

Secondly, the set-point temperature of **OptRef** ia slowly changing, so it gives a better result on humidity and control inputs compared to that of **Step** and **Trapz**. We show that abrupt changes of the set-point temperature in the case of **Step** can adversely disturb the zone humidity. The zone relative humidity in the case of **Step** and **Trapz** slightly change in the opposite direction to the set-point temperature while that of **OptRef** is well regulated.

Thirdly, with the relaxation of the constraint on the volumetric flow rate, we observe that the PMV in the case of **Step** and **Trapz** is greater than 0.5. On the other habd, applying **OptRef** along with specific volumetric flow rate to the HVAC system gives the PMV within 0.5.

In case of **OptRef**, the heat exchanger electrical power during off-peak period is slightly lower than that of the other cases. However, the dehumidifier uses a large control input to remove the same amount of the zone humidity. The reason is that the volumetric flow rate is greater than that of the case of **Step** and **Trapz**. Furthermore, we observe that **OptRef** gives a smoother electrical power profile while **Step** gives another peak of the electrical power when the set-point temperature returns to its nominal level. Therefore, employing **OptRef** would make the HVAC system have a longer lifetime and minimize the maintenance cost.

Last but not least, the supervisory control takes about 10 ms to compute **OptRef** and the average computing time of the MPC is 31 ms per iteration. In comparison to the sampling time of the MPC layer, it confirms that the proposed design can be applied to the real-time application.

On the other hand, there are some disadvantages on our control design. First

of all, one of the disadvantages is that the maximum benefit of the proposed design method relies on perfect weather and disturbance forecast. For another disadvantage, we observe that tracking error using **OpfRef** is generally larger than those of the other set-points due to its time-lag behavior.

4.6 Summary

In this chapter, we show the numerical results of the proposed control design including dynamic model, analysis of PMV, control design, and illustrative cases. In our illustrative cases, we show that our control objectives, namely, energy minimization and thermal comfort regulation, can be succesfully achieved by the proposed control design. Next, peak-load shaving, one major part to reduce energy consumption, can be done efficiently by **OptRef**. In addition, thermal comfort is well-regulated even if the weather conditions are changed. Furthermore, we point out interesting points in terms of discussion. Finally, we state advantage and disadvantage of using supervisory MPC.

CHAPTER V

CONCLUSIONS AND FUTURE WORK

5.1 Conclusions

In this thesis, we present a novel design of supervisory MPC for HVAC system that concerns both peak-load shaving and thermal confort.

In Chapter 1, we introduce research background of an HVAC system, thermal comfort, and a supervisory MPC. We state our research problem, objectives, and contributions.

In Chapter 2, we present a complex dynamic model of building HVAC system adapted from [25] which consists of temperature dynamics and humidity dynamics. We show that CFD model can be integrated to analyze air velocity inside the room. After that, we linearize nonlinear HVAC model around its equilibrium and implement a linearized model in the supervisory MPC.

In Chapter 3, we explain a formulation of the proposed supervisory MPC based on linearized model in Chapter 2. For the supervisory control, we apply TOC, TCC, and analysis of PMV properties to formulate the optimal set-point design problem. For the MPC layer, we search for the optimal control input satisfactory with our control objectives, namely, reference tracking and control input minimizing.

In Chapter 4, we investigate for application of the proposed control design in Chapter 3 and present illustrated examples. The simulations are done based on Thailand's weather condition, namely, summer season, rainy season, and winter season. We also compare the optimal set-point with the conventional set-point from our previous work [24]. As results, our numerical results reveal that the optimal set-point from the proposed control design works well resulted in better control on zone temperature, zone

humidity and zone PMV. Electrical power of heat exchanger is smoothly shaved in all simulations as well as TOC is reduced. Thermal comfort is well-regulated in an acceptable region. Moreover, we investigate performance of the proposed control design when the weather conditions are varied. Our results confirm that the proposed supervisory MPC succesfully handles various types of disturbance profile and yields a better results compared to conventional set-point design.

5.2 Recommendations for Future work

1. Extension of the single zone building to the multi-zone building is challenging due to a growth of computational cost. In addition, the electricity consumed by the other appliances, for example, lightning system, should be taken into account of electricity consumption of the building. This would show a possibility and a feasibility to implement the proposed control strategy in a real application.

2. The proposed control scheme provides good control results when disturbances data is accessible. Therefore, combination of the proposed control system with a acculate prediction system of weather data is highly recommended. Additionally, the prediction system would allow us to perform a long-term computation using the proposed control strategy.

3. The relaxation of a nonlinear model using linearization allows us to interpret the results analytically. However, this would make the design not applicable for other operating point. To improve this point, we suggest that an extension of the linear MPC to nonlinear one can be applied to the proposed control strategy.

4. PMV, which is used as the thermal comfort indicator, is used to determine the desired bound for set-point temperature and volumetric flow rate. [19] presented that the PMV can be directly included in the MPC constraint with linearzation techniques. This allows us to concern the level of the PMV straightforwardly.

Bibliography

[1] Trading Economics, "Thailand GDP." [Online]. Available: https://tradingeconomics.com/thailand/gdp, Accessed on Nov. 6, 2019.

[2] Energy Policy and Planning Office, Ministry of Energy. "Electricity Energy Consumption in Metropolitan Area Classified by Tariff." [Online]. Available:http://www.eppo.go.th/index.php/en/en-energystatistics/electricity-statistic?orders, Accessed on Nov. 4, 2019.

[3] P. K. Narayan and R. Smyth, "Multivariate Granger Causality between Electricity Consumption, Exports and GDP: Evidence from a Panel of Middle Eastern Countries," Energy Policy, vol. 37, no. 1, pp. 229–236, 2005.

[4] C. Magazzino, "Electricity Demand, GDP, and Employment: Evidence from Italy," Frontiers in Energy, vol. 8, no. 1, pp. 31–40, 2014.

[5] C. C. Lee, "Energy Consumption and GDP in Developing Countries: a Cointegrated Panel Analysis," Energy Economics, vol. 27, no. 3, pp. 415–427, 2005.

[6] S. T. Chen, H. I. Kuo, and C. C. Chen, "The Relationship Between GDP and Electricity Consumption in 10 Asian Countries," Energy Policy, vol. 35, no. 4, pp. 2611–2621, 2007.

[7] M. Shafie-khah, P. Siano, J. Aghaei, M. A. S. Masoum, F. Li, and J. P. S. Catalão, "Comprehensive Review of the Recent Advances in Industrial and Commercial DR," IEEE Transactions on Industrial Informatics, vol. 15, no. 7, pp. 3757-3771, Jul. 2019.

[8] N. Yamtraipat, J. Khedari, J. Hirunlabh, and J. Kunchornrat, "Assessment of Thailand Indoor Set-point Impact on Energy Consumption and Environment," Energy Policy, vol. 34, no. 7, pp. 765–770, 2006.

[9] M. H. Albadi, and E. F. El-Saadany, "A Summary of Demand Response in Electricity Markets," Electricity Power System Research, vol. 78, no. 11, pp.

1989–1996, 2008.

[10] P. Palensky and D. Dietrich, "Demand Side Management: Demand Response, Intelligent Energy Systems, and Smart Loads," IEEE Transactions on Industrial Informatics, vol. 7, no. 3, pp. 381–388, 2011.

[11] P. O. Fanger, Thermal Comfort: Analysis and Application in Environmental Engineering, McGraw-Hill New York, 1972.

[12] ASHRAE Standard 55: Thermal Environmental Conditions for Human Occupancy, ASHRAE, 2013.

[13] S. Wang and Z. Ma, "Supervisory and Optimal Control of Building HVAC System: A Review," HVAC & R Research, vol. 14, no. 1, pp. 3–32, 2008.

[14] L. Wang, Model Predictive Control System Design and Implementation Using MATLAB, 1st ed., Springer, New York, NY, USA, 2009.

[15] M. Maasoumy and A. Sangiovanni-Vincentelli, "Total and Peak Energy Consumption Minimization of Building HVAC Systems Using Model Predictive Control," IEEE Design & Test of Computers, vol. 29, no. 4, pp. 26–35, 2012.

[16] A. Afram and F. Janabi-Sharifi, "Theory and Applications of HVAC Control System–A Review of Model Predictive Control (MPC)," Building and Environment, vol. 72, pp. 343–355, 2014.

[17] M. Hu, F. Xiao, J. B. Jørgensen, and S. Wang, "Frequency Control of Air Conditioners in Response to Real-time Dynamic Electricity Prices in Smart Grids," Applied Energy, vol. 242, no. 1, pp. 92–106, Mar. 2019.

[18] C. Chen, J. Wang, and S. Kishore, "MPC-Based Appliance Scheduling for Residential Building Energy Management Controller," IEEE Transaction on Smart Grid, vol. 4, no. 3, pp. 1401–1410, Sep. 2013.

[19] J. Cigler, S. Prívara, Z. Váňa, E. Žáčeková, and L. Ferkl, "Optimization of Predicted Mean Vote Index within Model Predictive Control Framework: Computationally Tractable Solution," Energy and Buildings, vol. 52, pp. 39–49, 2012.

[20] J. Figueiredo and J. Sá da Costa, "A SCADA System for Energy Management in Intelligent Buildings," Energy and Buildings, vol. 49, pp. 85–98, 2012.

[21] A. Afram and F. Janabi-Sharifi, "Supervisory Model Predictive Controller (MPC) for Residential HVAC Systems: Implementation and experimentation on archetype sustainable house in Toronto," Energy and Buildings, vol. 154, pp. 268–282, 2017.

[22] J. Mei and X. H. Xia, "Energy-efficient Predictive Control of Indoor Thermal Comfort and Air Quality in a Direct Expansion Air Conditioning System," Applied Energy, vol. 195, pp. 439-452, 2017.

[23] J. Mei and X. H. Xia, "Distributed Control for a Multi-evaporator Air Conditioning System," Control Engineering Practice, vol. 90, pp. 85–100, 2019.

[24] C. Anuntasethakul and D. Banjerdpongchai, "Model Predictive Control Strategy Based on Predicted Mean Vote for Building HVAC System," in Proc. of 2019 SICE Annual Conference (SICE 2019), pp. 1386–1391, Sep. 2019.

[25] B. Tashtoush, M. Molhim, and M. Al-Rousan, "Dynamic Model of an HVAC System for Control Analysis," Energy, vol. 30, no. 10, pp. 1729–1745, 2005.

[26] B. Arguello-Serrano and M. Velez-Reyes, "Nonlinear Control of a Heating, Ventilating, and Air Conditioning Systems with Thermal Load Estimation," IEEE Transactions on Control Systems Technology, vol. 7, no. 1, pp. 56–63, 1999.

[27] R. B. Bird, E. N. Lightfoot, and W. E. Stewart, Transport Phenomena, 2nd ed., John Wiley & Sons, New Jersey, NJ, USA, 2002, pp. 78–80.

[28] K. T. Fong, T. T. Chow, C. Li, Z. Lin, and L. S. Chan, "Effect of Neutral Temperature on Energy Saving of Centralized Air-Conditioning Systems in Subtropical Hong Kong," Applied thermal Engineering, vol. 30, pp. 1659–1665, 2010.

[29] S. Zhang, Y. Cheng, Z. Fang, C. Huan, Z. Lin, "Optimization of Room Air Temperature in Stratum-ventilated Rooms for Both Thermal Comfort and Energy Saving," Applied Energy, vol. 204, pp. 420–431, 2017.

[30] Y. Deng, Z. Feng, J. Fang, S. Cao, "Impact of Ventilation Rates on Indoor Thermal Comfort and Energy Efficiency of Ground-source Heat Pump System," Sustainable Cities and Society, vol. 37, pp. 154–163, 2018.

[31] K. Ogata, Modern Control Engineering, Prentice Hall Upper Saddle River, New Jersey, NJ, USA, 2009.

[32] J. Nocedal and W. Stephen, Numerical Optimization, Springer, New York, NY, USA, 2006.

[33] H. Park, J. Sun, S. Pekarek, P. Stone, D. opila, R. Meyer, I. Kolmanovsky, and R. DeCarlo, "Real-Time Model Predictive Control for Shipboard Power Management Using the IPA-SQP Approach," IEEE Transactions on Control Systems Technology, vol. 23, no. 6, pp. 2129-2143, Nov. 2015.

[34] S. Matthew, "Human Body Heat as a Source for Thermoelectric Energy Generation," Physics 240, Fall, 2013, [Online]. Available: http://large.stanford.edu/courses/2016/ph240/stevens1/, Accessed on Dec. 23, 2019.

[35] MATLAB version 9.6.0.1214997 (R2019a) Update 6, The MathWorks, Inc., Natick, Massachusetts, 2019.

[36] Thailand Metropolitan Electricity Authority, "Time of Use Tariff for Medium General Service (in Thai)," [Online]. Available: https://www.mea.or.th/profile/109/113, Accessed on May 30, 2019.

BIOGRAPHY

Chanthawit Anuntasethakul was born in Bangkok, Thailand. He recieved his Bachelor degree in electrical engineering from Chulalongkorn University, Thailand, in 2018. In 2018, he began his research study at Control System Laboratory (CSRL), Department of Electrical Engineering, Faculty of Engineering, Chulalongkorn University, Thailand. Both undergraduate and graduate studies are supervised by Professor David Banjerdpongchai. His research interest consists of control system design, numerical optimization, and data analytic.

In connection to his thesis, he has the following publications.

1. C. Anuntasethakul, N. Techaphangam, and J. Songsiri, "A State-space Identification of Building Temperature System," in Proc. of *2018 15th International Conference on Electrical Engineering/Electronics, Computer, Telecommunications and Information Technology (ECTI-CON)*, pp. 66–69, 2018.

2. C. Anuntasethakul and D. Banjerdpongchai, "A Design of Integrated Real-time Optimization and PI Control for Building Temperature Control System," in Proc. of *2019 8th International Symposium on Design, Operation, and Control of Chemical Processes (PSE ASIA 2019)*, 2019.

3. C. Anuntasethakul and D. Banjerdpongchai, "Model Predictive Control Strategy Based on Predicted Mean Vote for Building HVAC System," in Proc. of *The SICE Annual Conference 2019 (SICE2019)*, pp. 1386–1391, 2019.

4. C. Anuntasethakul and D. Banjerdpongchai, "Design of Supervisory Model Predictive Control for Building HVAC System with Consideration of Peak-load Shaving and Thermal Comfort," *IEEE Access*, pp. 1–16, Mar. 2021, doi: 10.1109/ACCESS.2021.3065083.